Stability and characterization of GAP bonded ADN-propellant – the problem of gas formation during curing with isocyanates and characteristics of the glass-rubber transition

Manfred A. Bohn and Volker Gettwert

Fraunhofer Institut fuer Chemische Technologie, ICT, D-76318 Pfinztal, Germany

Abstract

During manufacturing of a GAP-ADN formulation in the framework of HISP - program [*]) a porous structure in the formulation was encountered. The pores are caused by gas formation during curing of the propellant mix. This is very disadvantages with respect to mechanical properties and burning behaviour. The conditions of pore formation and the possible causes should be clarified in order to avoid or at least to reduce the pore formation below a critical extent. The origin of the gas formation was assumed to be found in ADN itself or a reaction between ADN and the isocyanate Desmodur^{TM} E305, which was used to form the polyurethane based binder in the formulation. Gas evolution at several temperatures, 50°C, 60°C and 70°C as function of measurement time was applied to characterize the gas evolution rates. Besides Desmodur^{TM} E305 also the isocyanate IPDI (isophorone diisocyanate) was included in this investigation. The gas evolution was followed with two methods: by IR absorption of the concentration increase of N_2O (only with E305 because of to high vapour pressure of IPDI), a decomposition product of ADN and by total gas evolution using the vacuum stability apparatus equipped with pressure transducers. With IPDI also the anomalous decomposition behaviour of ADN was observed. The obtained results suggest that the reaction of ADN with isocyanate is the cause of the gas formation and that the control of temperature during propellant preparation, the mixing and especially the curing, plays a key role to avoid the formation of bubbles and pores in the cured formulation.

The so-named HISP 32 propellant (60 mass-% bimodal ADN (208µm and 55µm), 16 mass-% Al (18µm), 24 mass-% GAP diol binder with combined isocyanate and BPS curing) was further investigated to characterize its glass-rubber transition. For this dynamic mechanical analysis (DMA) in torsion mode was employed and the loss factor curve ($\tan\delta = G''/G'$) was analysed in terms of binder parts with different reorientational behaviour during the transition from glassy to rubbery state. The shape of the loss factor is composed of two transitions: the one at lower temperatures originates from the undisturbed binder part and the one on the higher temperature side is caused by mobility restrictions exerted on the binder by the fillers, here ADN and Al powder. The perspective is that the different binder parts are differently sensitive to external loads as ageing and strain rate.

[*]) HISP = High Performance Solid Propellants for In-space Propulsion.
HISP has received funding from the European Community's Seventh Framework Programme (FP7/2007-2013) under Grant Agreement No. 262099)

Paper 116, pages 116-1 to 116-27 in **CD-Proceedings** of the 46th International Annual Conference of ICT on 'Energetic Materials – Performance, Safety and System Applications', June 23 to 26, 2015, Karlsruhe, Germany. ISSN 0722-4087. Fraunhofer-Institut fuer Chemische Technologie (ICT), D-76318 Pfinztal. Germany.

1. Introduction

At time the common high-performance rocket propellants are based on an elastomeric binder containing as oxidizer AP (ammonium perchlorate) and as fuel besides the binder Al powder. The disadvantage is the production of HCl (hydrogen chloride) from AP, which is highly corrosive, loads platforms (strong corrosion on steel parts) and personal and causes undesired signature. Further on, AP produces increasing problems by contaminating drinking water. Perchlorate is very persistent in the environment because it is quite non-reactive. Further, the perchlorate anion is of very similar size as the iodide anion, and therefore perchlorate competes with iodide to be incorporated into the thyroid gland, which may degrade the proper functioning of it /1/. Therefore, a lot of effort was and is made to replace AP in order to get so-named 'green' propellants. Surely, one main driver is to reduce signature of the composite propellants. Also organic compounds are looked for as possible replacement oxidiser /2, 3/, for example the BTNEN (bis (trinitroethyl) nitramine), Figure 1, which has as HNF (hydrazinium nitroformate) the nitroform (trinitromethyl) group as the oxygen carrying group. This type of substance is named also high-energy dense oxidizers (HEDOs). It was investigated already quite early, more than 60 years ago /4/. The results on chemical stability are not satisfactory.

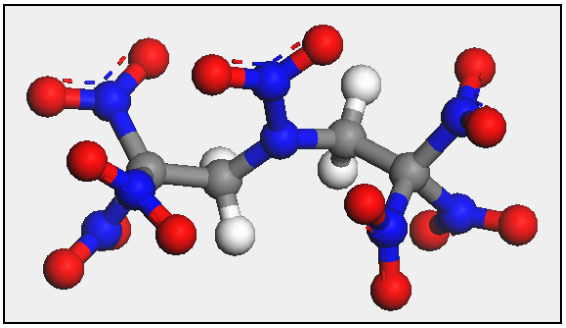

Figure 1: Structure of BTNEN (bis (trinitroethyl) nitramine), an organic oxidizer with OB =16.5%. The nitroform groups show the typical propeller conformation. (red = oxygen, blue = nitrogen, grey = carbon, white = hydrogen).

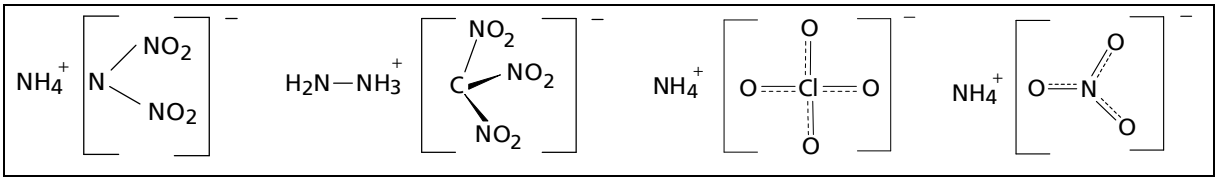

Figure 2: Chemical structure formulas of ADN (ammonium dinitramide), HNF (hydrazinium nitroformate), AP (ammonium perchlorate) and AN (ammonium nitrate) (from left to right). In the solid phase all four substances are present in ionic forms.

Table 1: Performance data of the oxidizers ADN, AP, AN and HNF. The values of the heats of explosion and gas volumes have been calculated by the ICT-Thermodynamic-Code. The other data are from the ICT-Thermochemical Data Base /7/.

Substance	molar mass	O_2-balance	enthalpy of formation ΔH_f^0		Q_{EX} *)	density	gas vol. *]	T_M
	[g/mol]	[%]	[kJ/mol]	[J/g]	[J/g]	[g/cm³]	[cm³/g]	[°C]
ADN	124.056	+ 25.8	– 149.8	– 1207.5	3337	1.81	592	92.9
AP	117.489	+ 34.0	– 295.8	– 2517.7	1972	1.95	533	150; D
AN	80.043	+ 20.0	– 365.6	– 4567.5	2479	1.73	459	169.9
HNF	183.081	+ 13.1	– 76.9	– 420.0	5579	1.91	568	124; D

*) Q_{EX} heat of explosion, with reaction water as liquid (25°C), the value represents thermodynamically controlled combustion;
*] gas volume at 25°C, 1 bar without water, for thermodynamically controlled combustion;
D in the column of T_M (melting temp.) means decomposition at the given temperature, which may vary with the sensitivity of the observation.
Decomposition of AP: in adiabatic selfheating determined by ARC and phi-factor ϕ= 10.4 the onset of recognized decomposition was 210°C. But one must say that the decomposition could start earlier first with lower ϕ-factor and before 210°C the decomposition seems to be endothermal.

Meanwhile a lot of work was dedicated into the investigation of HNF and ADN: decomposition behaviour of ADN, the stabilization of ADN, use of ADN in propellants and decomposition and burning behaviour of HNF and some investigations in model-type propellants [see recent review article, 5, 6]. Figure 2 shows the chemical structures of ADN, HNF, AP and AN. In Table 1 some basic performance data are listed.

As conclusion from all the results the following can be said. Between ADN and HNF there is a difference in chemical stability, which could be named fundamental. First the intrinsic stability of ADN is significantly higher than the one of HNF. The decomposition of ADN is very probably triggered by protonation of the dinitramide anion. When this protonation is hindered, ADN is highly stable in solid state with activation energies of decomposition well beyond 220 kJ/mol. The protonation can be hindered easily by adding substances capturing protons.
HNF decomposes much faster than ADN and faster than non-stabilized nitrocellulose. However the main feature of HNF decomposition is the intrinsic production of highly reactive species as nitrenes and carbenes. These species are so reactive that they immediately make insertion reaction in some neighbouring bond, means of what is just nearby. Added substances in usual amounts of 1 to 2 mass-% are practically without any effect in capturing theses reactive species. In other words: HNF is not stabilizable /5, 6/.
Other problems exist with HNF. One is the compatibility with other ingredients. ADN is not free of problems in this regard, but HNF is superior in incompatibility. Finally, HNF formulations have a not benign burning behaviour. All attempts to get an acceptable pressure exponent n in the burning law of Vieille failed so far /8/.

2. Investigation of gas generation from reaction of ADN with isocyanate

2.1 Investigation of evolved gases by IR-Analysis

In cured propellant formulation pores were formed by gas formation and for this the probable causes are:

- Humidity
  H_2O reacts with the isocyanate group R-NCO under formation of CO_2 coming from the NCO-group, which is finally converted to an amine functionality R-NH_2;
  The amine in turn reacts readily with R-NCO to urea functionalities
  R-NH-C(=O)-NH-R
- Reaction of ADN with R-NCO
  The formation of N_2O originates from ADN and CO_2 from the NCO group. In experiments the formation of N_2O and CO_2 was confirmed by EGA (evolved gas analysis) by FTIR (Fourier Transform Infrared) from mixtures of ADN and R-NCO, see Figure 1.

The analysis cell was purged and filled with argon. The determined CO_2 is therefore not atmospheric CO_2.

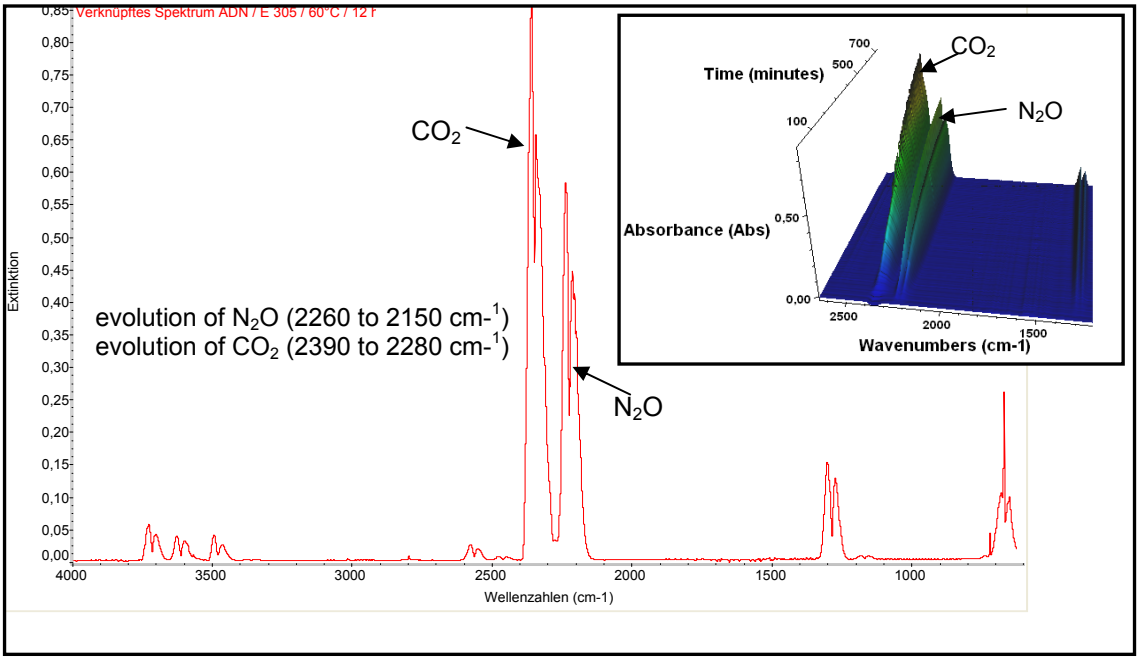

Figure 1: Formation of CO_2 and N_2O by reaction between ADN and isocyanate (Desmodur™ E305) in an EGA (Evolved Gas Analysis) cell. The cell was purged and filled with argon.

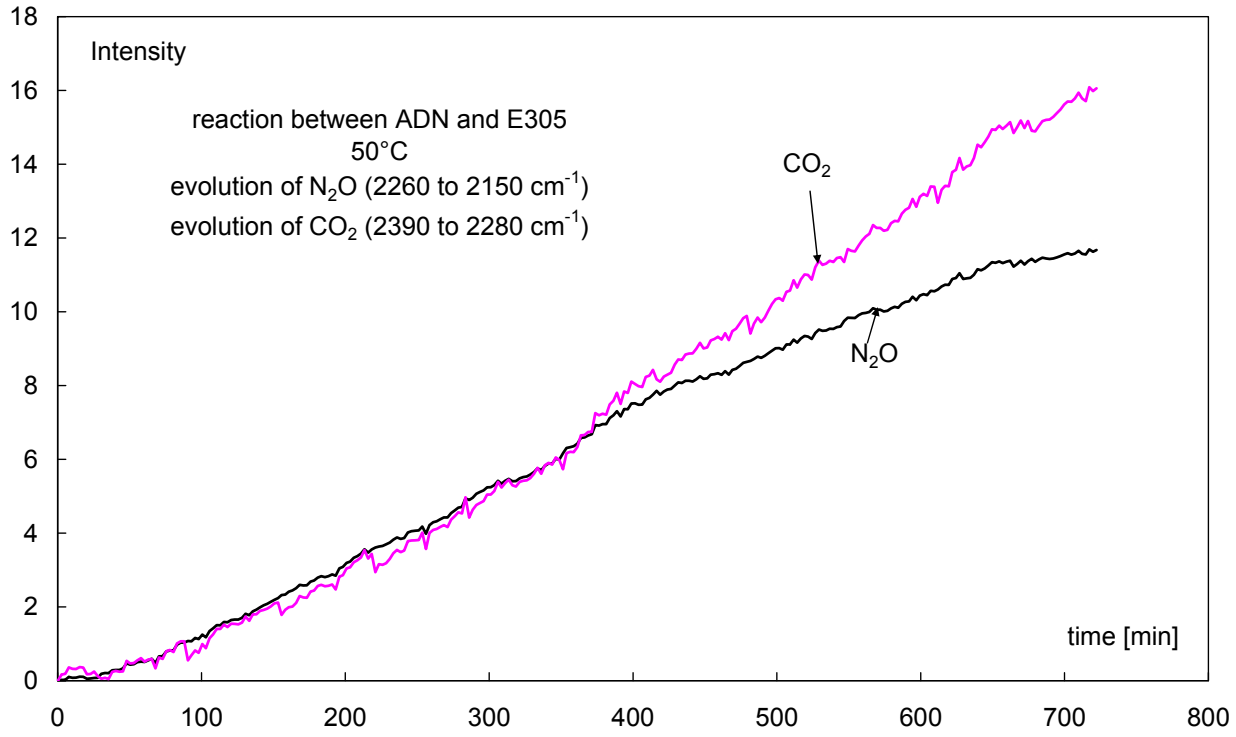

Figure 2: Evolution of N_2O and CO_2 from the reaction of ADN and isocyanate Desmodur™ E305 at 50°C. Up to 400 min the evolution of both gases is fairly parallel. Then the evolution of CO_2 is faster.

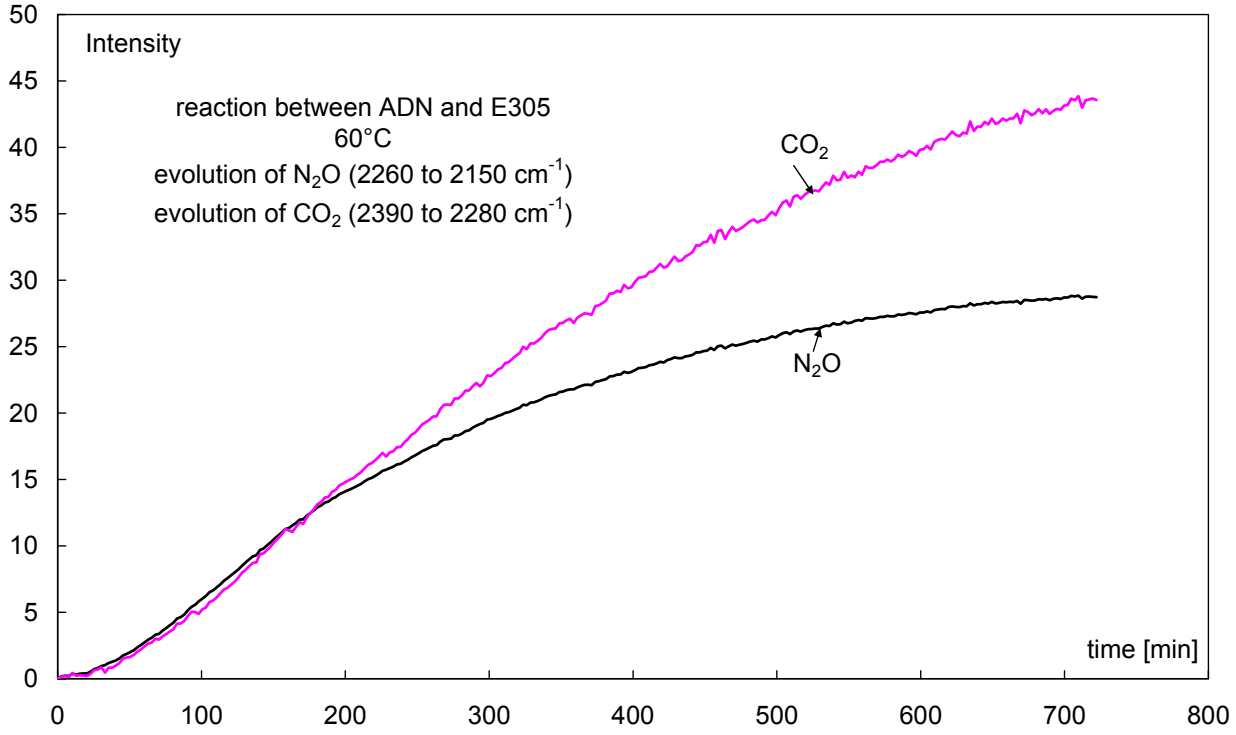

Figure 3: Evolution of N_2O and CO_2 from the reaction of ADN and isocyanate Desmodur™ E305 at 60°C. Up to 200 min the evolution of both gases is fairly parallel. Then the evolution of CO_2 is faster.

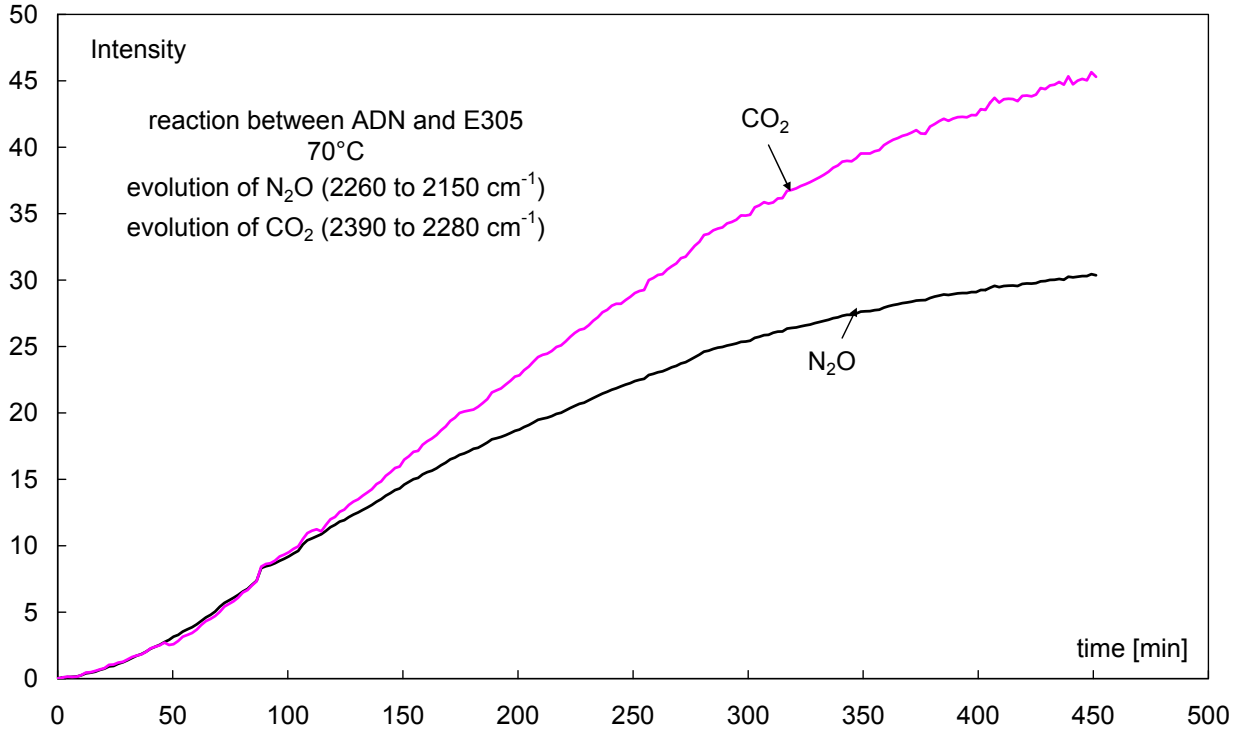

Figure 4: Evolution of N_2O and CO_2 from the reaction of ADN and isocyanate Desmodur™ E305 at 70°C. Up to 140 min the evolution of both gases is fairly parallel. Then the evolution of CO_2 is faster.

In the Figures 2 to 4 the evolution of CO_2 and N_2O is shown at the temperatures 50°C, 60°C and 70°C. In all three cases the N_2O formation goes in parallel with CO_2 in an initial time interval. Its length is temperature dependent. Then CO_2 develops always faster than N_2O. In the following a hypothesis is given to explain this behaviour. Further on it seems that the residual humidity of ADN is not a critical point, because CO_2 is not formed in surplus to N_2O during the initial reaction time periods.

The standard thermal decomposition reaction of ADN is into N_2O and NH_4NO_3 (ammonium nitrate).

$$NH_4{\cdot}N(NO_2)_2 \longrightarrow N_2O + NH_4NO_3$$

In the presence of isocyanate the parallel formation of N_2O and CO_2 was confirmed by EGA analysis. The N_2O is liberated from ADN and CO_2 should come from the NCO group. A possible reaction could be the following, it is a hypothesis.

$$NH_4{\cdot}N(NO_2)_2 + R\text{-}N{=}C{=}O \longrightarrow R-\bar{\underline{N}} + CO_2 + N_2O + NH_4NO_2$$

The R-NCO-group forms thereby a nitrene, which reacts immediately by insertion reaction, by itself or with neighbouring substances.

A further possibility for CO_2 production would be the oxidation of the carbon skeleton of the isocyanate. But then also CO should probably appear. The reaction with isocyanate therefore reduces ADN and NH_4NO_2 (ammonium nitrite) is formed instead of ammonium nitrate. The NH_4NO_2 is a quite instable substance and decomposes readily into N_2 and two H_2O.

$$NH_4NO_2 \longrightarrow N_2 + 2\,H_2O$$

This decomposition gives rise to further gas formation and additional CO_2 production by the reaction of water with the isocyanate. This explains the increased CO_2 formation against N_2O formation, as shown in the above Figures. Further on it shows that the gas production is quite effective and the formation of pores is accelerated.

In the following some mechanistic reaction pathways are presented, which can be considered as alternative to the above reactions. The ones of Figure 7 form at the end CO_2 and N_2O. In Figure 5 the reactions of H_2O and NH_3 with isocyanate are shown. In Figure 6 the reaction of isocyanate with an amine function is given, whereby a urea type is formed, which can react further with isocyanate to form biuret.

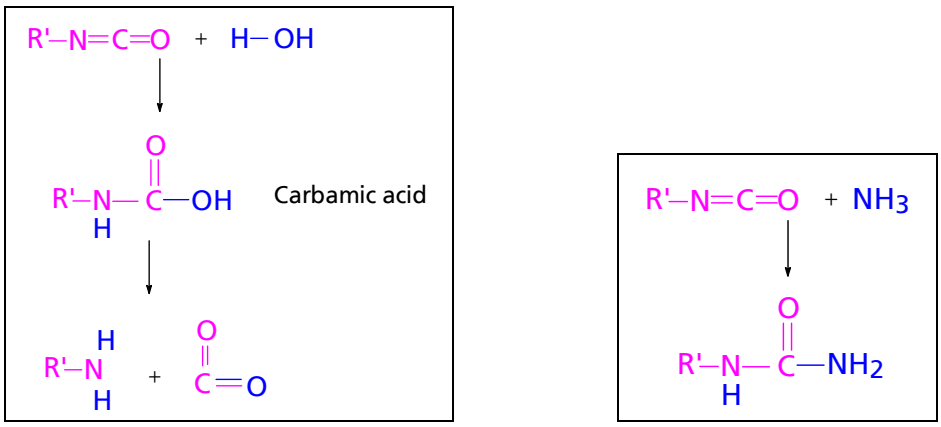

Figure 5: Left side: reaction of water with isocyanate gives the intermediate carbamic acid, which is not stable and decomposing in amine and CO_2. Right side: Reaction of NH_3 with isocyanate gives a urea.

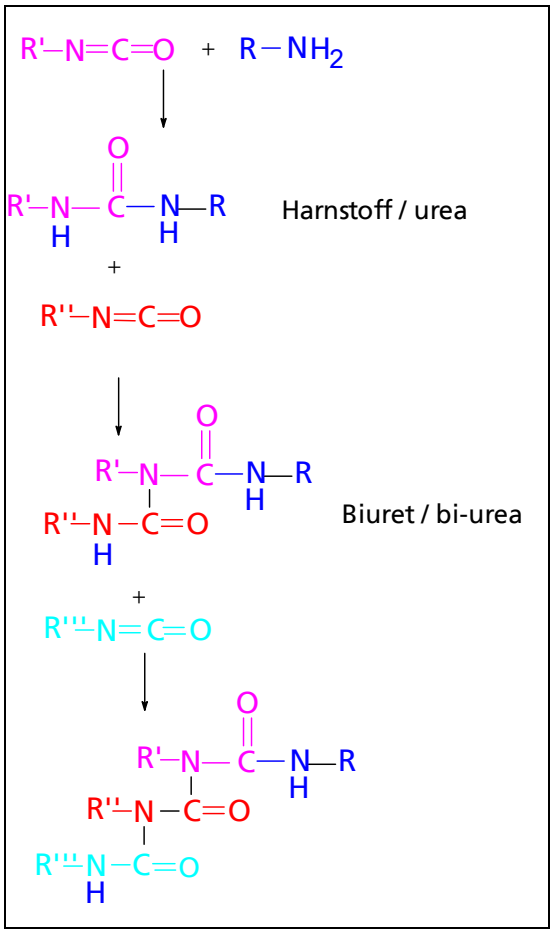

Figure 6: Reaction of isocyanate with an amine function forms urea. Further reaction of urea with isocyanate forms biuret (bi-urea). This reaction may continue to give finally a polymeric product.

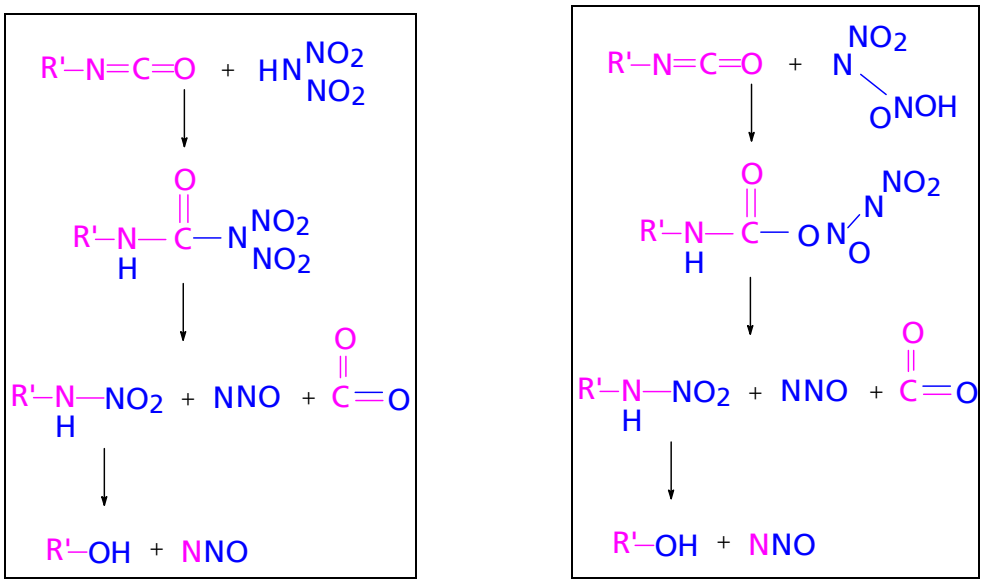

Figure 7: Reaction of isocyanate with dinitramine acid formed from ADN, by removing NH_3 by another isocyanate molecule. Left side: reaction with one isomeric form of HDN, right side: reaction with another isomeric form of HDN. In both cases finally N_2O (two molecules) and CO_2 and an alcohol are formed. The alcohol reacts again with isocyanate to form a urethane.

2.2 Investigation by total gas generation followed by the OZM-VST apparatus

The tracing of gas evolution by IR-analysis is only in part quantitative because one can follow only gas molecules with IR-active vibrations. Nitrogen for example cannot be followed. Therefore the method of measuring the evolution of all gaseous components was employed. For this purpose the typical methods to follow quantitatively the gas generation used in vacuum stability testing (VST) can be applied. In this case the most suitable method is the pressure transducer method, produced by the Czech company OZM.

Another question is does ADN show anomalous decomposition with R-NCO? Anomalous decomposition was found by the group around Manelis /9/. They showed that ADN decomposes around 60°C faster than according to the Arrhenius behaviour, when the rate constants are extrapolated from higher temperatures (90°C) down to 50°C / 40°C. The typical temperature of occurrence of anomalous behaviour is between 65°C and 60°C.

Figure 8 shows the gas evolution of two lots of ADN prills alone at 80°C up to 6 days or about 140 h. To get the values for 70°C, 60°C and 50°C, these data have to be divided by 3, 9 and 27, respectively. This means the gas generation of pure ADN alone is very low and can be neglected. The vapour pressures of the isocyanates were not higher than the ones of the ADN prills.

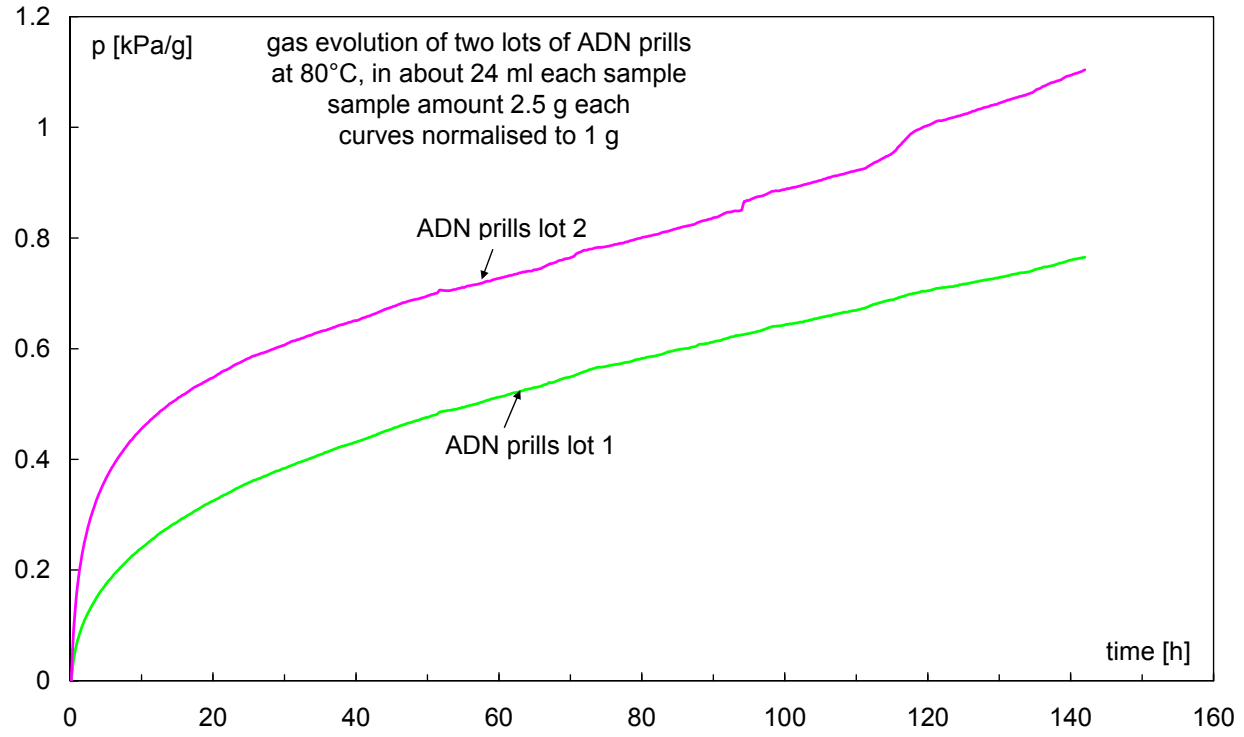

Figure 8: Gas evolution of two lots ADN prills determined at 80°C. To have the values for 70°C, 60°C and 50°C, these data have to be divided by 3, 9 and 27, respectively. The normalised final gas volumes are (0°C, 1 atm): 0.17 ml/g and 0.21 ml/g after 142h.

In the first investigation series the IPDI (isophorone diisocyanate) was used together with ADN. The IPDI could not be used with the IR-analysis; because of its relatively high vapour pressure, which caused a high IR opaqueness in the IR measurement cell. With the OZM-VST no problems have arisen from this point. The ADN-IPDI mixtures were 2:1 by mass means two parts of ADN and one part of IPDI. Results are available for 50°C, 60°C and 70°C. The measured gas evolution curves are shown in the Figures 9, 10 and 11. In Figure

12 an overview can be seen. For evaluation, the data from the 50°C and 70°C measurements were corrected formally to 60°C measurement tube temperature (according to ideal gas behaviour) in order to be directly comparable with the data from the 60°C measurement. Also a correction to 0°C for all three temperatures could be done.

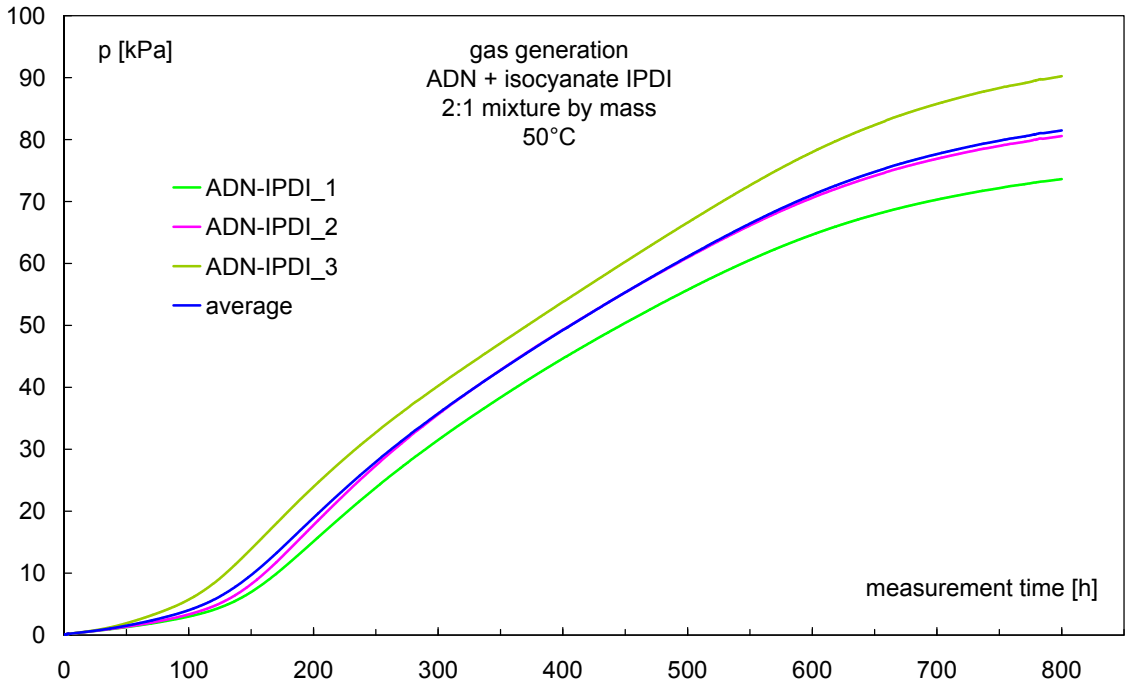

Figure 9: Following the decomposition of ADN + IPDI by gas generation at 50°C. Three samples in parallel. Sample amount about 0.5g each, pressure development in about 24 ml each. The normalised final gas volume is (0°C, 1 atm): 37.3ml/g after 812 h.

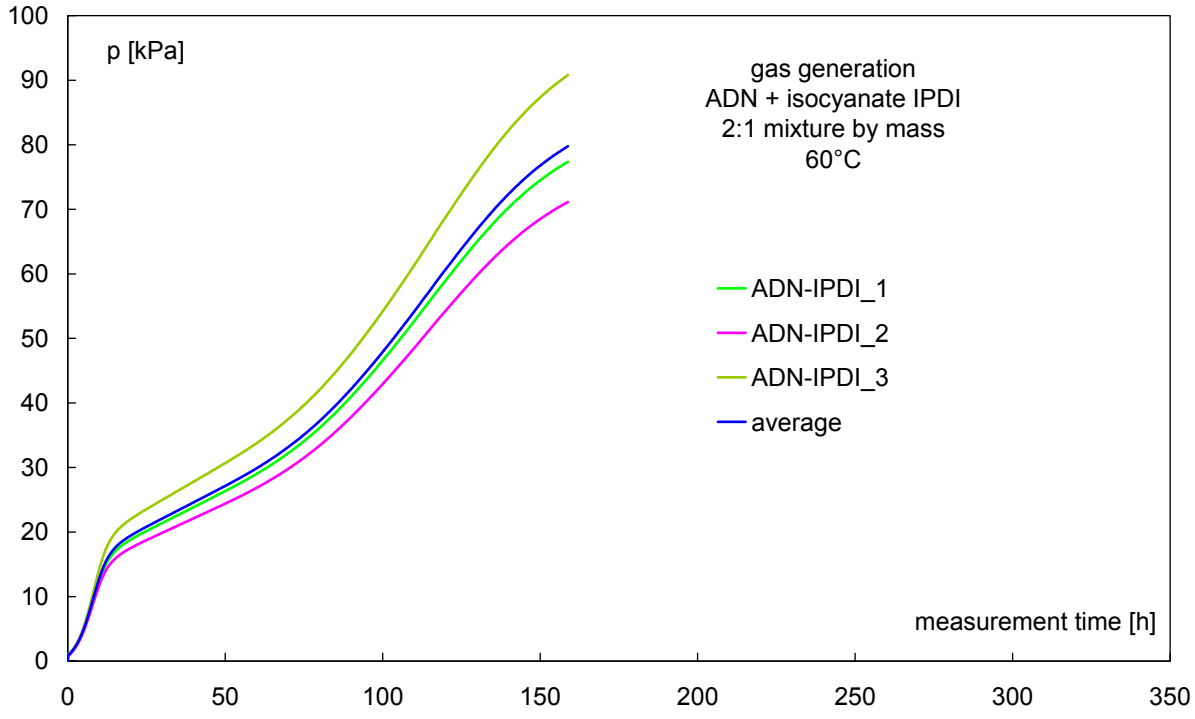

Figure 10: Following the decomposition of ADN + IPDI by gas generation at 50°C. Three samples in parallel. Sample amount about 0.5g each, pressure development in about 24 ml each. The normalised final gas volume is (0°C, 1 atm): 32.4ml/g after 137.5 h.

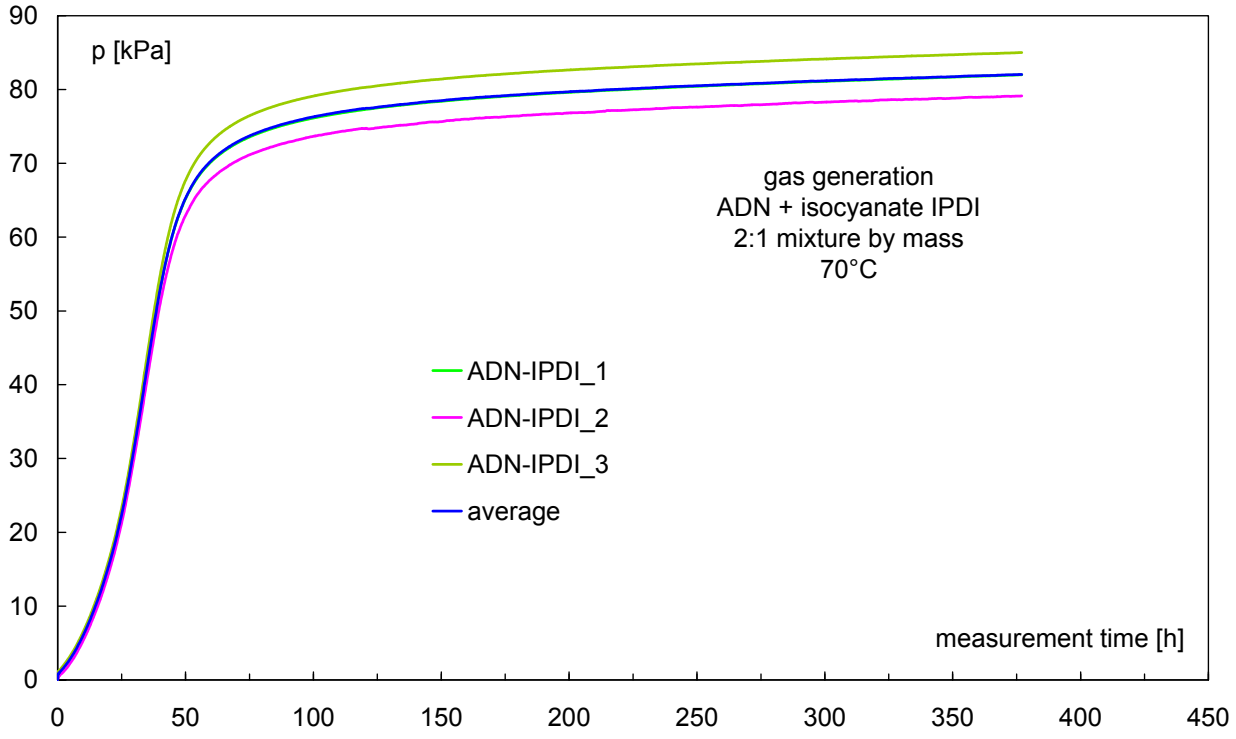

Figure 11: Following the decomposition of ADN + IPDI by gas generation at 70°C. Three samples in parallel. Sample amount about 0.5g each, pressure development in about 24 ml each. The normalised final gas volume is (0°C, 1 atm): 33.3ml/g after 382 h.

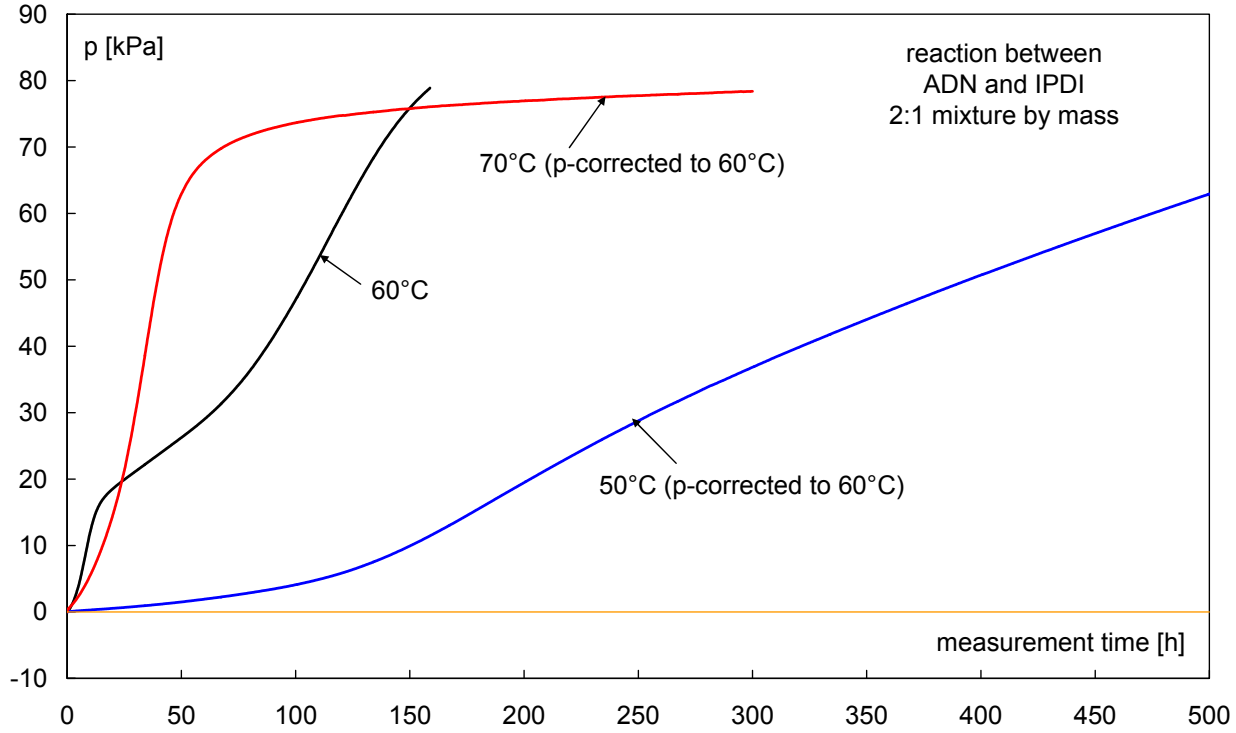

Figure 12: Comparison of the gas generations at 50°C, 60°C and 70°C. The data from the 50°C and 70°C measurements were corrected for 60°C tube temperature in order to be directly comparable with the data from the 60°C measurement.

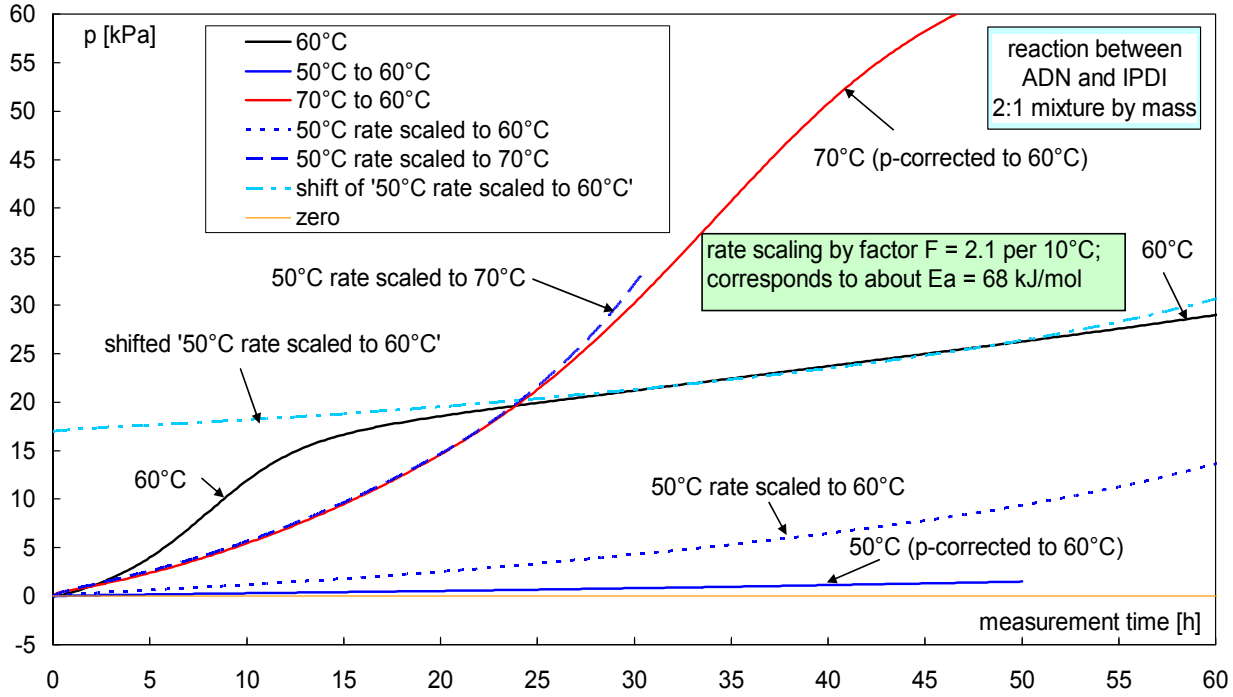

Figure 13: Comparison of gas evolution data and extrapolation of the 50°C measurement to 60°C and 70°C by the generalized van't Hoff rule.

With the data presented in the Figure 13 several items are discussed. First one can recognize that at the beginning of the reaction, during the first 25 hours, the gas evolution at 60°C is higher than at 70°C. This can be assigned to the anomalous decomposition behaviour of ADN as it was reported in /9/. Later on the decomposition slows down. The reason for this is the return to normal decomposition behaviour after the production of some reaction products as amines and water, which disturb the ADN in such a way that anomalous decomposition is no longer favoured. The second item is the scaling of the gas generation rate at 50°C to the other two temperatures.

$$F_{\Delta T} = \approx \exp\left(+\frac{Ea}{R}\cdot\frac{\Delta T}{T^2}\right) \qquad (1)$$

Table 2: Converting factor F from van't Hoff equation to Ea values and vice versa using Eq.(1). The ΔT is the temperature difference for which F is valid; here always 10°C is used.

ΔT [°C]	10	
Ea [kJ/mol]	70	
R [J/mol/K]	8.31441	
T [°C]	T [K]	F
30	303.15	2.5
40	313.15	2.36
50	323.15	2.24
60	333.15	2.14
70	343.15	2.04
80	353.15	1.96
90	363.15	1.89
100	373.15	1.83
110	383.15	1.77

ΔT [°C]	10	
F	2.1	
R [J/mol/K]	8.31441	
T [°C]	T [K]	Ea [kJ/mol]
30	303.15	56.7
40	313.15	60.5
50	323.15	64.4
60	333.15	68.5
70	343.15	72.6
80	353.15	76.9
90	363.15	81.4
100	373.15	85.9
110	383.15	90.6

Pseudo gas generations at 60°C and at 70°C obtained out of the 50°C data were established. For this scaling the generalized van't Hoff rule was taken and its factor F was set to 2.1, for details see /10, 11/ and the following section. The scaling of the 50°C data to 70°C fits the measured data at 70°C. But the scaled 50°C data to 60°C is far away from measured data at 60°C. However, in shifting these scaled data along the ordinate by 17 kPa, one finds a reasonable agreement with the 60°C data, after the initial period, where the anomalous decomposition was active. This proves the return to normal decomposition behaviour. The value of F=2.1 corresponds to an activation energy of 68 kJ/mol, see the evaluations in Table 2, whereby Eq.(1) was used for conversion from F to Ea and vice versa. Such low activation energies are typical for isocyanate reactions. Also the polyurethane formation has Ea values in this range.

2.3 Generalized van't Hoff rule

The base of the generalized van't Hoff (GvH) rule is old van't Hoff rule known to every chemist: The increase or decrease of temperature by 10°C increases or decreases the reaction rate constants by an average factor F of 3; mostly the range is between 2 to 5. This factor was established by Jacobus Henricus van't Hoff (* August 30, 1852 in Rotterdam; † March 1, 1911 in Berlin-Steglitz). He was a chemist from The Netherlands. The data for this rule were created during his time in Berlin, Germany, where he worked from 1896 on until he died there. This rule should not be confused with the van't Hoff equation or van't Hoff law, Eq. (2), which is also know as reaction isobar, because it is valid at constant pressure. The formal identity with the temperature dependence of the Arrhenius equation is not accidental. There is the strong hint that Arrhenius has taken this van't Hoff law and applied it in the analogous form to the temperature dependence of the reaction rate constants.

The functioning of the generalized van't Hoff (GvH) rule is shown in Eq.(3) to Eq.(5). In Eq.(3) the rate equation is shown, formulated according to van't Hoff. Eq.(4) shows the ratio of two rates and the resulting time ratio. Eq.(5) is the worked out GvH, formulated for the relation between test times t_T and in-service time t_E with corresponding temperatures T_T and T_E. All the quantities used are explained in the legend of Eq.(5). For preset in-service conditions the corresponding test conditions can be obtained and vice versa.

$$\left(\frac{d\ln(K_E(T))}{dT}\right)\Big|_p = \frac{\Delta H}{R \cdot T^2} \qquad (2)$$

$$k(T) = H \cdot F^{(T/\Delta T_F)} \qquad (3)$$

$$\frac{k_2(T)}{k_1(T)} = F^{(+(T_2-T_1)/\Delta T_F)} = \frac{t_1(T)}{t_2(T)} \qquad (4)$$

$$t_T[d] = t_E[a] \cdot F^{-(T_T-T_E)/\Delta T_F} * 365.25$$

$$t_E[a] = t_T[d] \cdot F^{+(T_T-T_E)/\Delta T_F} / 365.25 \qquad (5)$$

1 year = 365.25 days (averaged with leap years)
1 month = 365.25 / 12 = 30.44 days
t_E in-use time in years at temperature TE
t_T test time in days at test or ageing temperature TT

T_T test or ageing temperature
T_E in-use temperature
F acceleration or deceleration factor per 10°C temperature change
ΔT_F temperature interval assigned to actual value of factor F, mostly 10°C

The GvH is especially effective in cases where two reaction mechanisms with different activation energies take place. Examples are the decomposition of NC-based materials and the oxidation of the HTPB binder or similar material with double bonds. We will first have a look on the situation for NC-based materials, Fig. 14. For heat generation rate of NC-based materials the used two mechanisms have activation energy values of 120 kJ/mol at higher temperatures and 80 kJ/mol at lower temperatures, whereby a sharp switch is taken at 60°C to facilitate the description, see STANAG 4582 and AOP 48. The real combined reaction rate constant is shown in Fig.14 as the red curve. In Fig. 15 the GvH is applied for this situation, shown as green curve. This green curve coincides nearly completely with the red curve. In conclusion: the GvH describes very good NC-based material showing the two-mechanistic decomposition behaviour. The Fig. 16 represents the situation with the times as function of temperature. Also here the GvH gives the correct description. In Fig. 17 the situation for HTPB binder can be seen. It was found that the oxidation reaction of this binder follows a two mechanistic reaction behaviour /10 and literature there/. The activation energies are somewhat different for HTPB compared to NC. Also here the GvH gives the correct description and can therefore be used to establish ageing plans as it was shown in /12/.

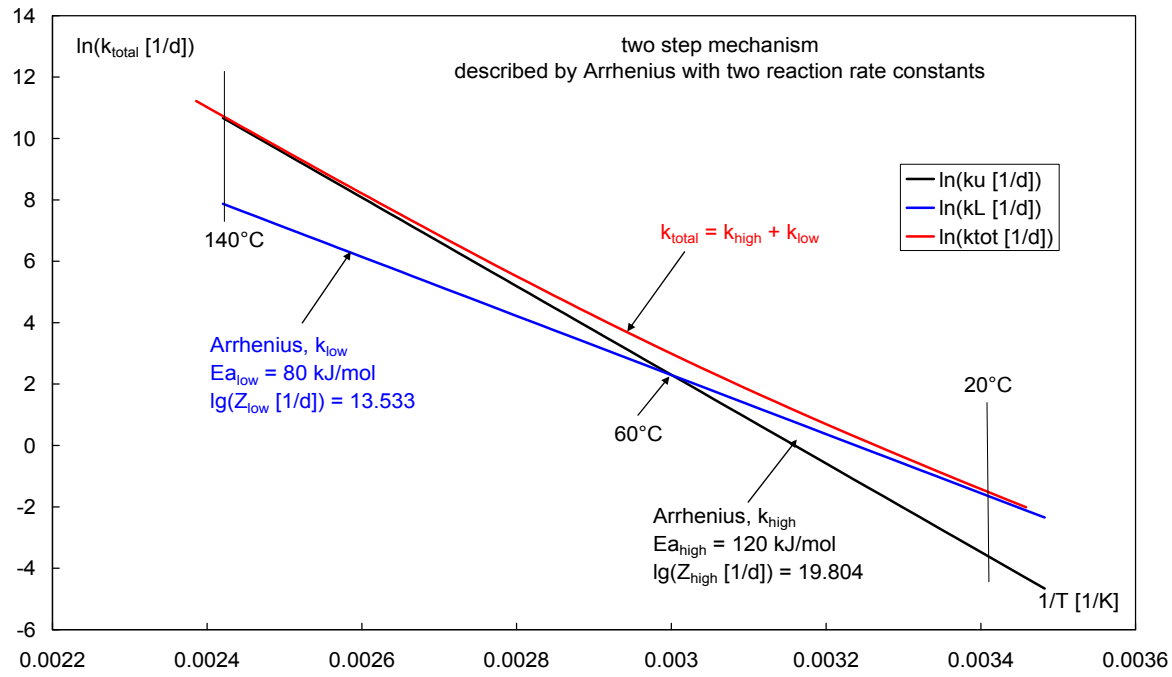

Figure 14: Illustration of the condition of a two mechanistic reaction behaviour as used in STANAG 4582 and AOP 48 for heat generation rate measurements and stabilizer assessment with NC-based energetic materials. The red curve is the actual apparent rate constant.

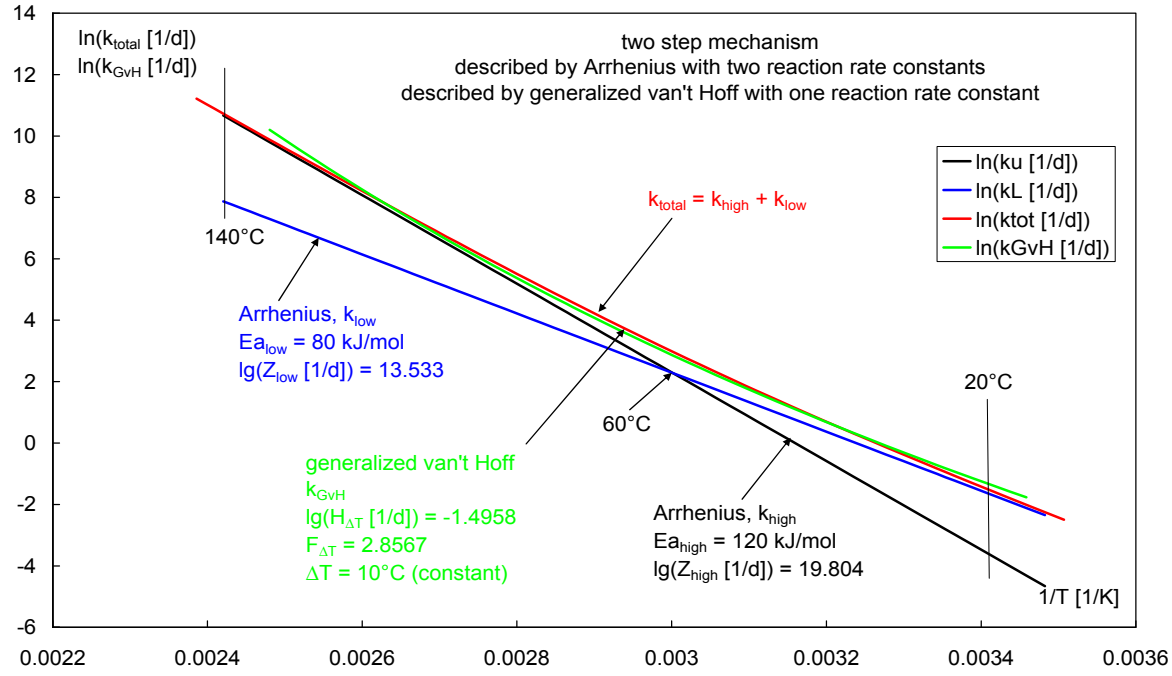

Figure 15: Application of the GvH to the two step mechanistic reaction behaviour used in STANAG 4582 and AOP 48. The green GvH line fits with F =2.86 quite well the red curve of the true rate constant in the interesting temperature range for NC-based material.

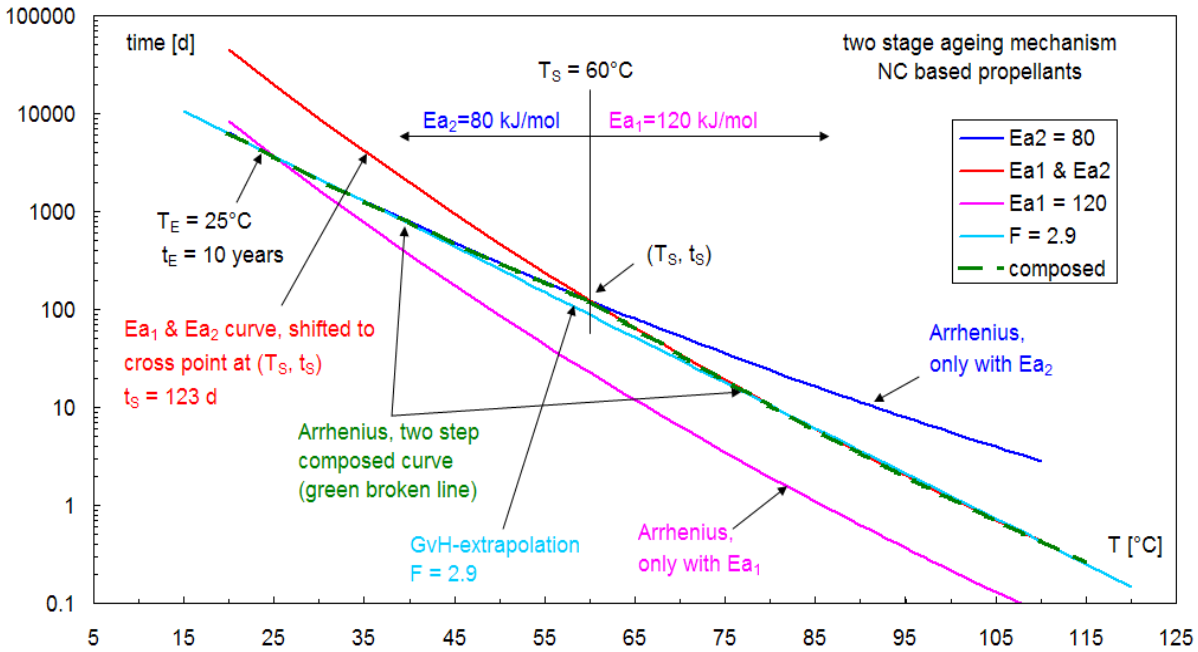

Figure 16: Application of the GvH to the two step mechanistic reaction behaviour used in STANAG 4582 and AOP 48, now for the times as function of temperature. The cyan GvH line represents the course of the true times with an F value of rounded to 2.9 per ΔT= 10°C.

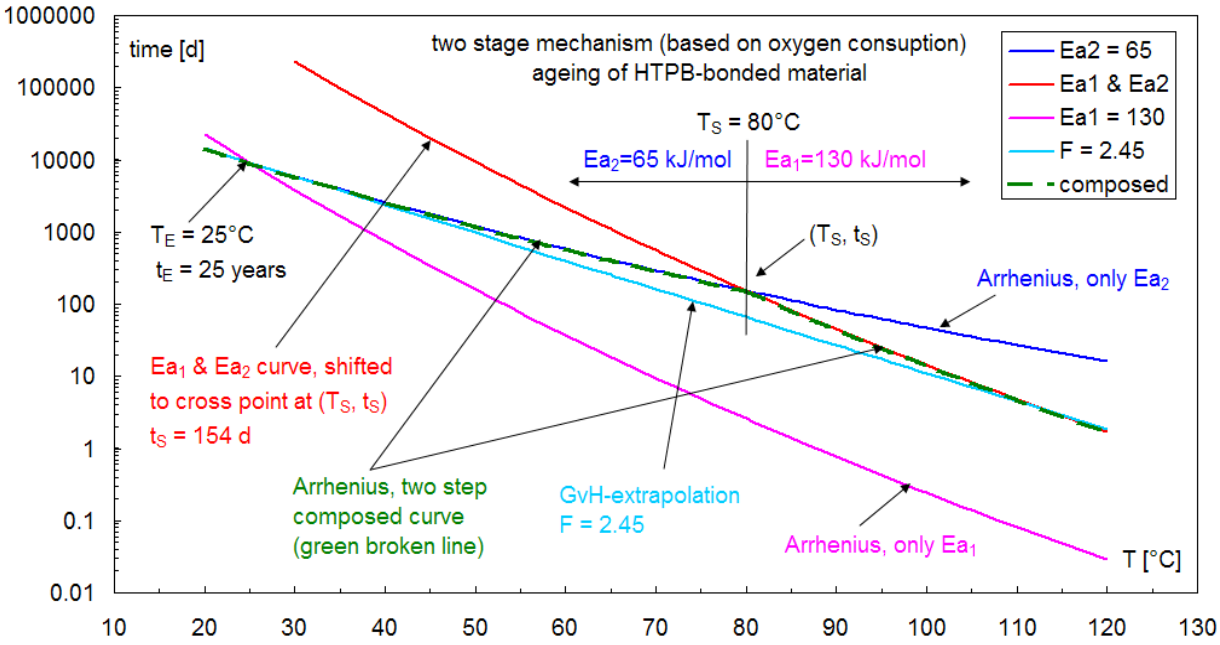

Figure 17: Application of the GvH to the two step mechanistic reaction behaviour found with the binder HTPB-IPDI, for the times as function of temperature. The cyan GvH line represents the course of the true times. Note the change in F value compared to NC-based material. Here the value is F=2.45 per ΔT=10°C.

3. Mechanical properties of ADN-propellant formulation HISP 32 as determined by torsion DMA

The RP formulation of ICT for the HISP program, the HISP 32 (see Abbreviations for details) with GAP based binder with combined curing by BPS and Desmodur™ E305, was subjected to DMA investigations with an instrument of type ARES™ from Rheometric Scientific, which measures in torsion mode. With this method, one analyses the mechanical behaviour in the linear viscoelastic range (this means the modulus is independent from the applied strain), by sinusoidal deformation at several deformation frequencies. The advantage of this method is to get information on the glass-rubber transition (GRT), which is a transition from energy elasticity (glassy state) to entropy elasticity (rubbery state) of an elastomer. With DMA the transition is probed by mechanical loading of the sample. In contrast, by using DSC, which may detect also this transition, the probing of the sample is by a thermal effect, namely the change in heat capacity over this transition, whereby the temperature of the maximum change of heat capacity is taken as glass-rubber transition temperature $T_{g,DSC,h}$. (the h means the heating rate used, because the transition temperature range depends on it). It is meanwhile a general experience that DMA probes the GRT more sensitive than DSC. This means the information about the transition is much more detailed and more precise with DMA than with DSC. Especially the reorientational transitions encountered in the polymer shell of the binder around the solid filler particles are not detected by DSC. Also so-named reptation movements (in principle possible, but very probably do not occur here, because of to high interaction energies between the chains) of not bonded GAP chains cannot be detected. Further on, the assigned temperature of the GRT is with DSC to low with respect to the strain rate shifting of this transition in the real cases of mechanical loading, which is in strain rate range of 100 Hz to 1000Hz.

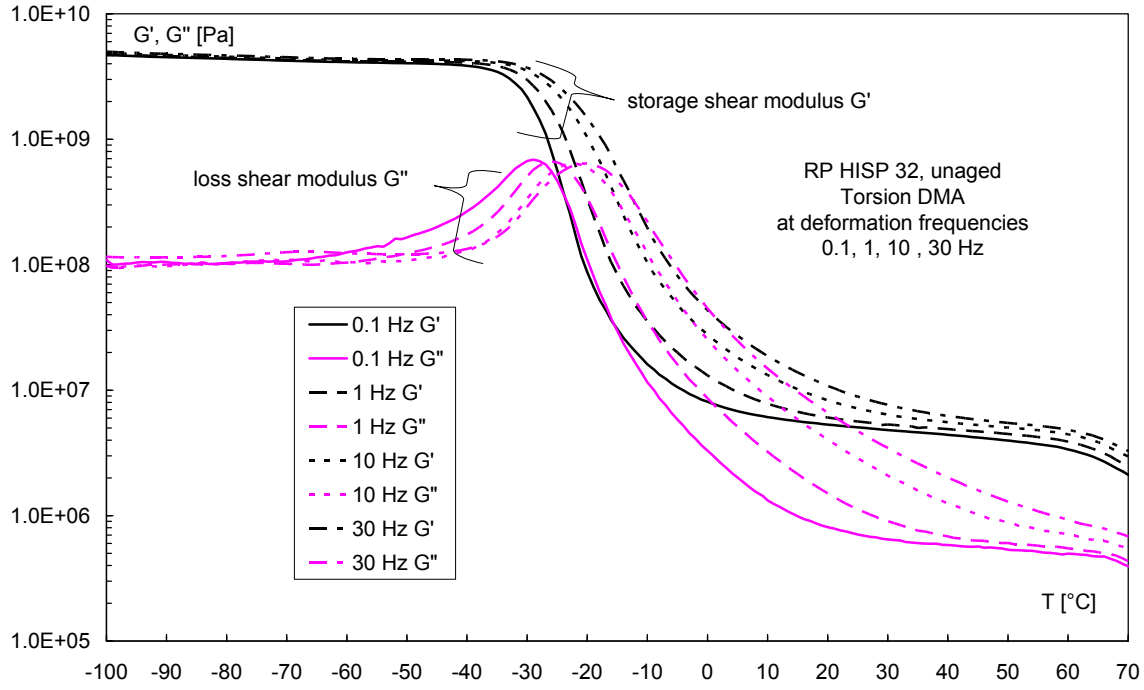

Figure 18: Torsion DMA measurements with RP formulation HISP 32. Shear storage modulus G′ and shear loss modulus G″ as function of measurement temperature and deformation frequency of sinusoidal sample loading.

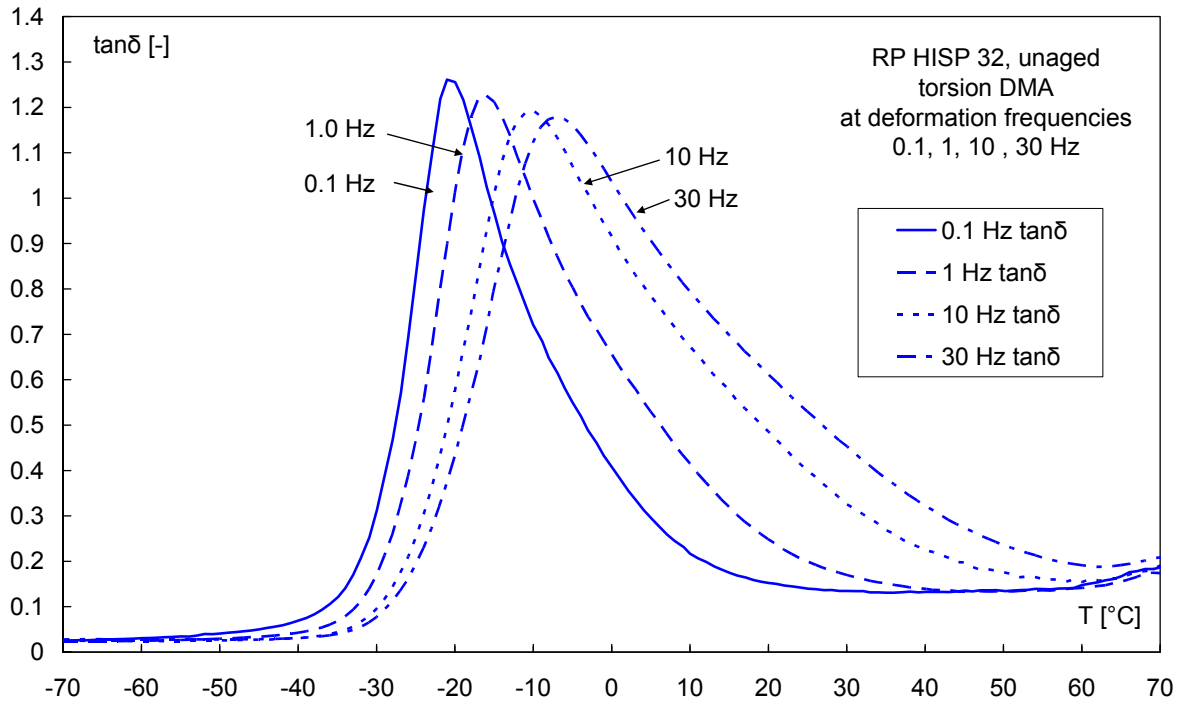

Figure 19: Torsion DMA measurements with RP formulation HISP 32. Loss factor tanδ =G″/G′ as function of measurement temperature and deformation frequency of sinusoidal sample loading, not baseline corrected.

In Fig. 18 the storage shear modulus G′ and the loss shear modulus G″ are shown as function of temperature and deformation frequency. The typical features to be expected from a rubbery material are shown. The corresponding loss factor tanδ = G″/G′ can be seen in Fig. 19. The maxima of these curves are taken as GRT temperatures $T_{g,DMA,f}$. Because the

peak position is dependent on deformation frequency, this parameter should/must be given in the data. With DSC one determines a $T_{g,DSC,h}$ at a specified heating rate h, mostly 10°C/min. This value corresponds to DMA peak position at a deformation frequency of about 0.001 Hz. Also DSC detects the transition represented by the maximum of loss factor and not by the maximum of the loss modulus, which is sometimes stated, because the maximum change in specific heat is during the rearrangement processes of the binder molecules. One recognizes the not symmetrical shape of the loss factor curves, an information not obtainable by DSC applying standard determination of $T_{g,DSC,h}$. Indeed, this shape of the loss factor is of importance to extract valuable information about the binder behaviour during the GRT.

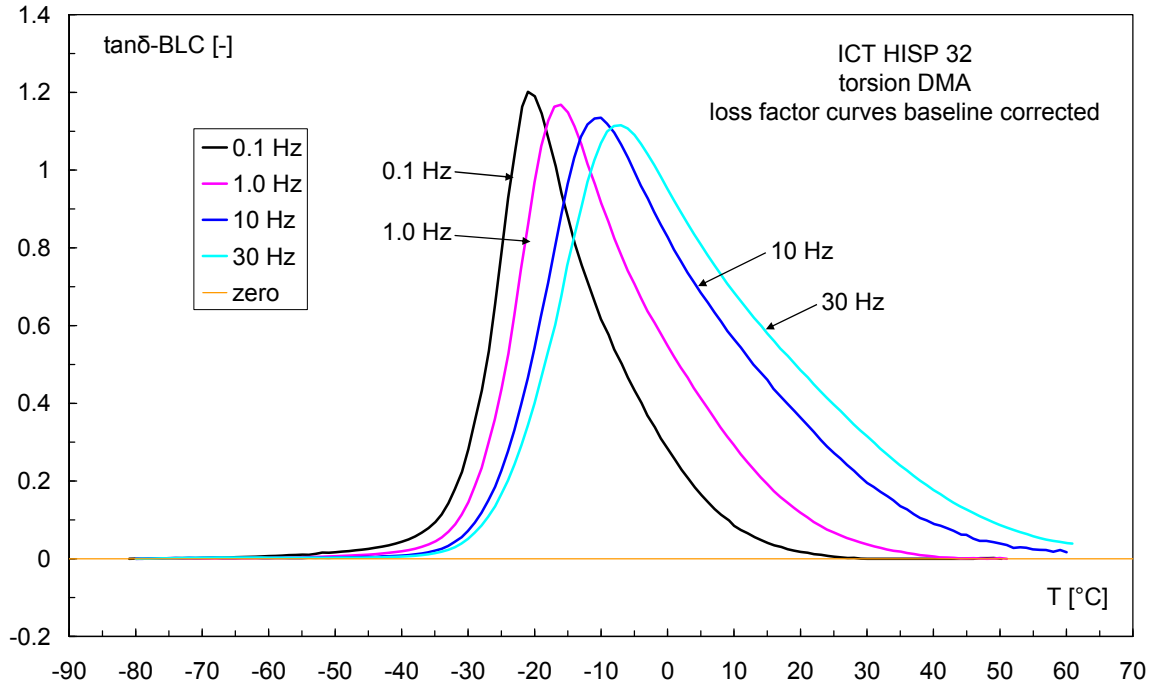

Figure 20: Loss factor tanδ =G″/G′ of RP formulation HISP 32 as function of measurement temperature and deformation frequency of sinusoidal sample loading, now the curves are baseline corrected.

Fig. 20 presents the so-named baseline corrected (BLC) loss factor curves. The baseline correction is done to separate the energy part used to perform the reorientation of the polymer molecules (in going from the energy to the entropy elasticity configurations) from such energy parts, which are used up just in frictional dissipative effects of the polymer. This last part is not of interest, because it is not used in a 'productive' way, mean for the reorientation, means to achieve the rubbery state. Only the parts of the loss factor curve which can be attributed to reorientational work will be considered further. The procedure to correct the baseline is shown in Fig. 21. It is in detail described in /12, 13, 14/. The choice of baseline is always an important point. Here the following is done. Assuming to have plateau values in the loss factor curve at both ends, a straight line could not describe the correct evolution of the baseline at the ends, because the baseline must appear out of the plateau at the lower temperature side and end on the other side into the plateau, means in both cases with a horizontal tangent. Such a quality of a baseline is achieved with a partitioning function α(T) shown in Eq.(6).

$$\alpha(T) = \frac{\int_{T_A}^{T} \tan\delta(T) \cdot dT}{\int_{T_A}^{T_B} \tan\delta(T) \cdot dT} \qquad (6)$$

This partitioning function uses the course of the loss factor curve to weight for each point of the baseline the transition from one end to the other of the loss factor curve. It is part of the actual baseline function BL_α given in Eq.(7).

$$BL_\alpha(T) = (1 - \alpha(T)) \cdot \tan\delta(T_A) + \alpha(T) \cdot \tan\delta(T_B) \qquad (7)$$

$BL_\alpha(T)$	baseline correction function between T_A and T_B, adjusted with α
$\alpha(T)$	normalised partitioning function of the $\tan\delta(T)$ curve
T_A	start temperature of the base line [°C]
T_B	end temperature of the base line [°C]
T	actual measurement temperature between T_A und T_B [°C]
$\tan\delta(T_A)$	$= a_1$ value of $\tan\delta(T)$ at T_A
$\tan\delta(T_B)$	$= a_2$ value of $\tan\delta(T)$ at T_B

The procedure is applied in loop until the change in loss factor curve is below a set convergence criterion Dk, Eq.(8).

$$D_k = \sum_{T_A}^{T_B} (\tan\delta\_I_{k-1}(T_i) - \tan\delta\_I_k(T_i))^2 \qquad (8)$$

D_k assessment parameter for the k^{th} iteration cycle, k = 1, 2, 3,…

The iteration of the baseline is always stable and fast in the usual cases.

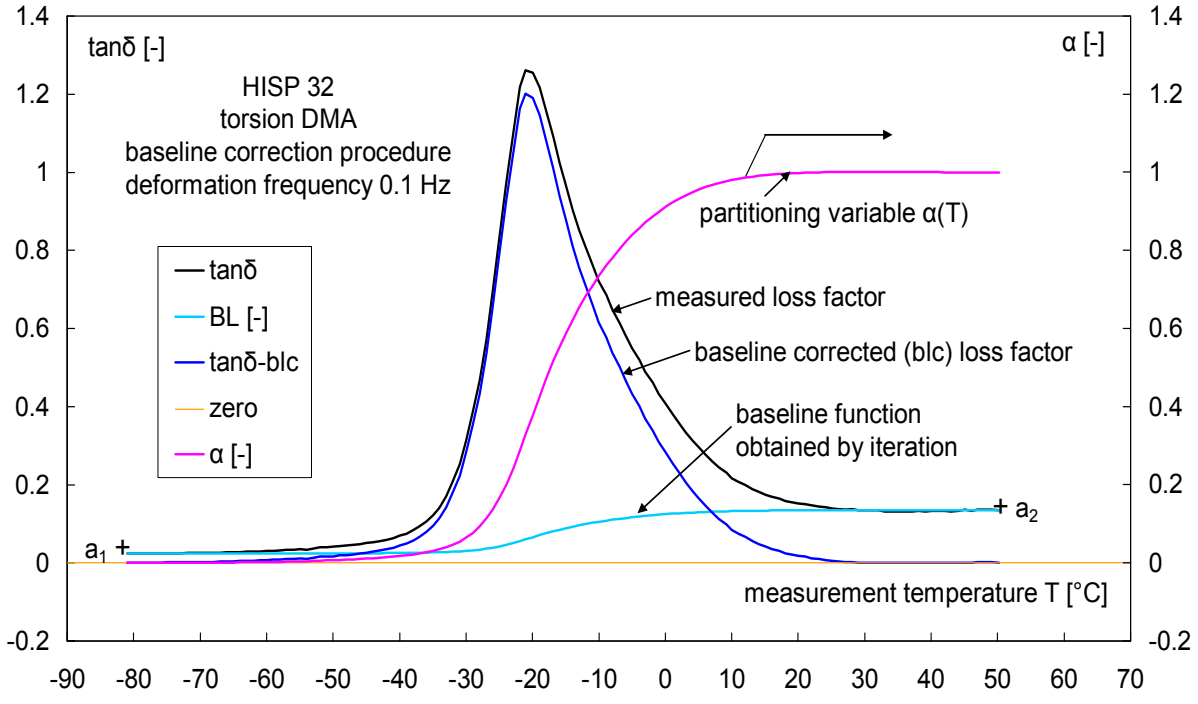

Figure 21: Illustration of baseline correction procedure on the loss factor tanδ =G"/G'.

The next step is to model the baseline corrected loss factor curve in order to separate the different binder mobilities expressed in the loss factor curve. To do this one can assume that the transition of an isotropic material follows a random distribution of the single transitions and should be describable by a gauss distribution function. Because the loss factor curves are not fully symmetrical a further dissipative relaxation happens, which can be described by exponential functions. Therefore an exponentially modified Gauss distribution (EMG) is used, Eq.(9). For a test of the quality of the assumption of a Gaussian distribution of the reorientational processes, only Gauss distributions are applied with Eq.(10).

$$\tan\delta_{BLC} = td_0 + \sum_{i=1}^{N} \frac{A_i}{\tau_i} \cdot \frac{1}{2} \cdot \exp\left[0.5 \cdot \left(\frac{w_i}{\tau_i} \right)^2 - \frac{T - Tc_i}{\tau_i} \right] \cdot \left\{ 1 - \mathrm{erf}\left[-\frac{1}{\sqrt{2}} \cdot \left(\frac{T - Tc_i}{w_i} - \frac{w_i}{\tau_i} \right) \right] \right\} \quad (9)$$

T measurement temperature, in [°C]
$\tan\delta_{BLC}$ value of tanδ after the baseline correction (BLC) as function of T; [-]
A_i peak area of the Gauss peak i, equivalent to area of the EMG peak I, in [°C]
w_i half peak width at half height of only Gaussian part, in [°C]
Tc_i temperature at peak maxima of Gaussian part of EMG (not the peak maxima of EMG), in [°C]
τ_i relaxation parameter in exponential part of EMG, also To is used, in [°C]
td_0 offset in tanδ data (here the value was fixed equal to 0), in [-]
N number of EMG fitting functions
erf in EMG equation means the error function.

$$\tan\delta_{BLC} = td_0 + \sum_{i=1}^{N} \frac{A_i}{w_i \cdot \sqrt{2\pi}} \cdot \exp\left[-0.5 \cdot \left(\frac{T - Tc_i}{w_i} \right)^2 \right] \quad (10)$$

The results of the modelling can be seen in Fig. 22 for the description with two Gauss distributions only. The modelling is already quite good and this confirms that the processes constituting the loss factor curve are really Gaussian processes. The description with Eq.(9) can be seen in Fig. 23. Qualitatively the result is similar to Fig. 22, but the correlation coefficient has improved, the description is better.

From the experience up to date with this type of modelling and the data description it is to be expected that the EMG at higher temperatures, means the right one in Fig. 23, is a sensitive indicator for ageing phenomena: hardening of the binder or softening of the binder, as well as for de-bonding /12, 15, 16/. But with HTPB-based propellants and ingredients catalysing the oxidation (iron catalysts for AP decomposition), the whole loss factor curve is strongly affected and the intensity of the loss factor can decreases severely /17/.

The transition at lower temperatures characterizes the mobility of the unrestricted binder part in the HISP 32 formulation. This peak has about one third of the total transition intensity. One can say one third of the binder is not mobility restricted by the filler particles Al and ADN. The other part is probably composed of two parts, because one can expect that ADN an Al form different binder shells. But the separation of them is not easy, because the structural information in the band shape of the loss factor curve may be not detailed enough.

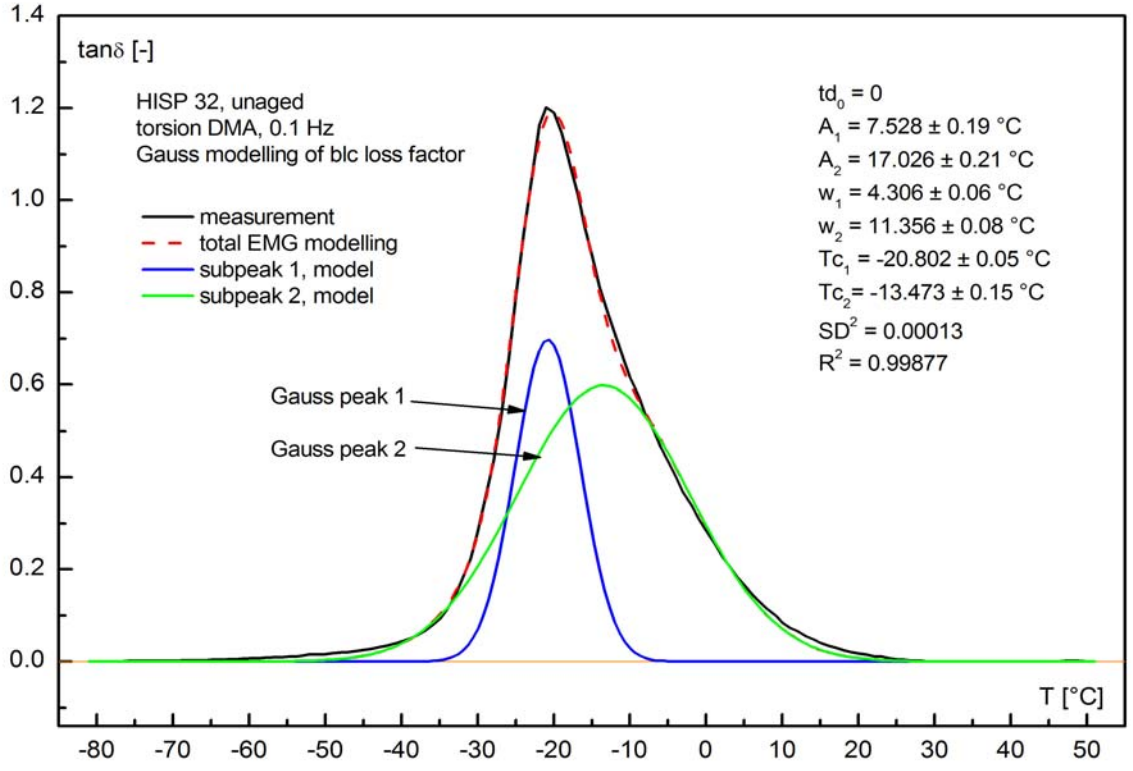

Figure 22: Modelling of the baseline corrected loss factor at 0.1 Hz deformation frequency of RP formulation HISP 32 only with two Gauss functions. Already with such a modelling the result is good.

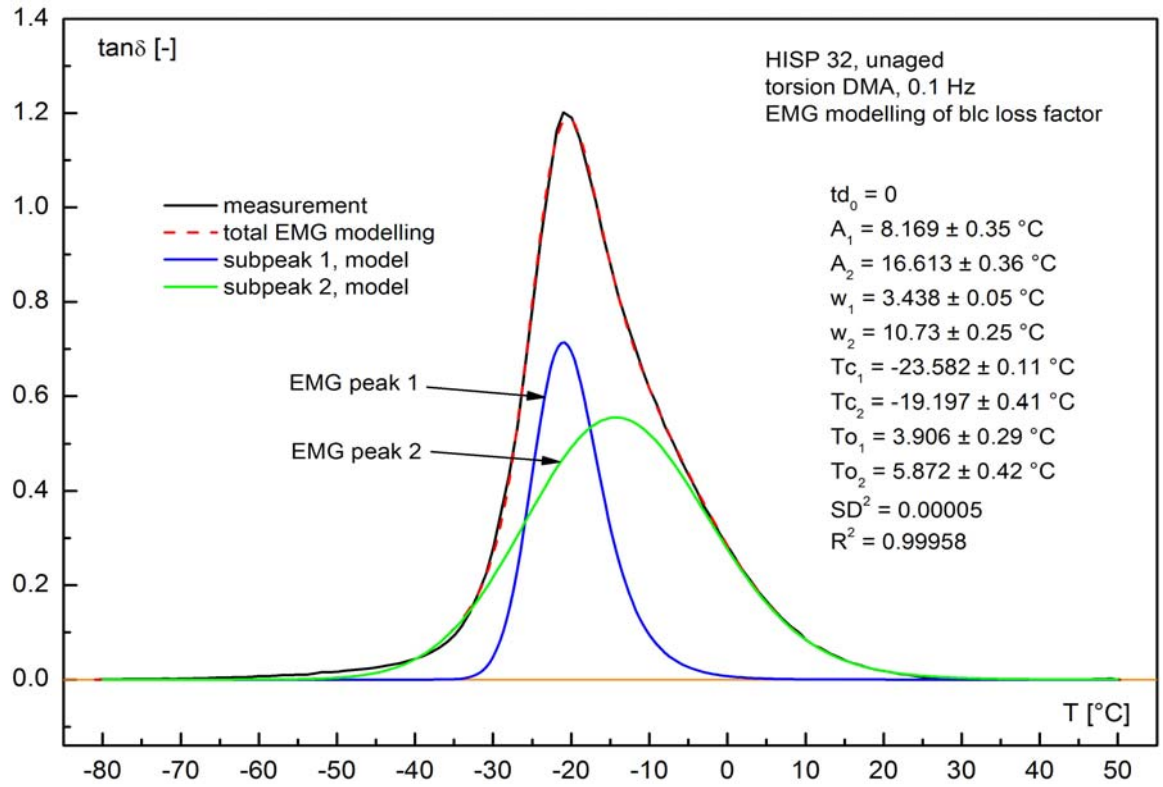

Figure 23: Modelling of the baseline corrected loss factor at 0.1 Hz deformation frequency of RP formulation HISP 32 with two EMG functions. The description is improved compared to the one with only two Gauss distributions.

Table 3: Temperatures of the maxima in G" and tanδ as function of deformation frequency f. It is pointed out that the difference in T_{max} between G" and tanδ increases with deformation frequency, means the peak of tanδ shifts 'faster' to higher temperatures than the one of G".

T_{max} in G''		T_{max} in tanδ		Deformation frequency f		Difference in T_{max} (G'' – tanδ)
T_{max} [°C]	$1/T_{max}$ [1/K]	T_{max} [°C]	$1/T_{max}$ [1/K]	ln(f [Hz])	f [Hz]	ΔT_{max}
-28.84	0.00409316	-20.61	0.00395977	-2.3025851	0.1	-8.23
-25.89	0.00404433	-16.32	0.00389363	0	1	-9.57
-22.4	0.00398804	-10.59	0.00380865	2.30258509	10	-11.81
-20.46	0.00395742	-7.37	0.00376251	3.40119738	30	-13.09
350 ± 12		239 ± 12		Ea_f [kJ/mol]		
73.78 ± 2.65		48.545 ± 2.57		$lg(Z_f$ [Hz])		
0.9974		0.9943		R^2		

Another important point to characterize the binder material is the shift with deformation frequency of the peak maximum temperatures of loss factor tanδ and the ones of loss modulus G", which are due to strain rate hardening. There is a saying that the glass temperature determined from DMA measurements is the maximum of the loss modulus, whereby deformation frequency has to be specified. Clearly to say the reorientation of the molecules happen in the range of the loss factor. Therefore to characterize the glass-rubber transition the temperature of the maximum of the loss factor is the suitable property.

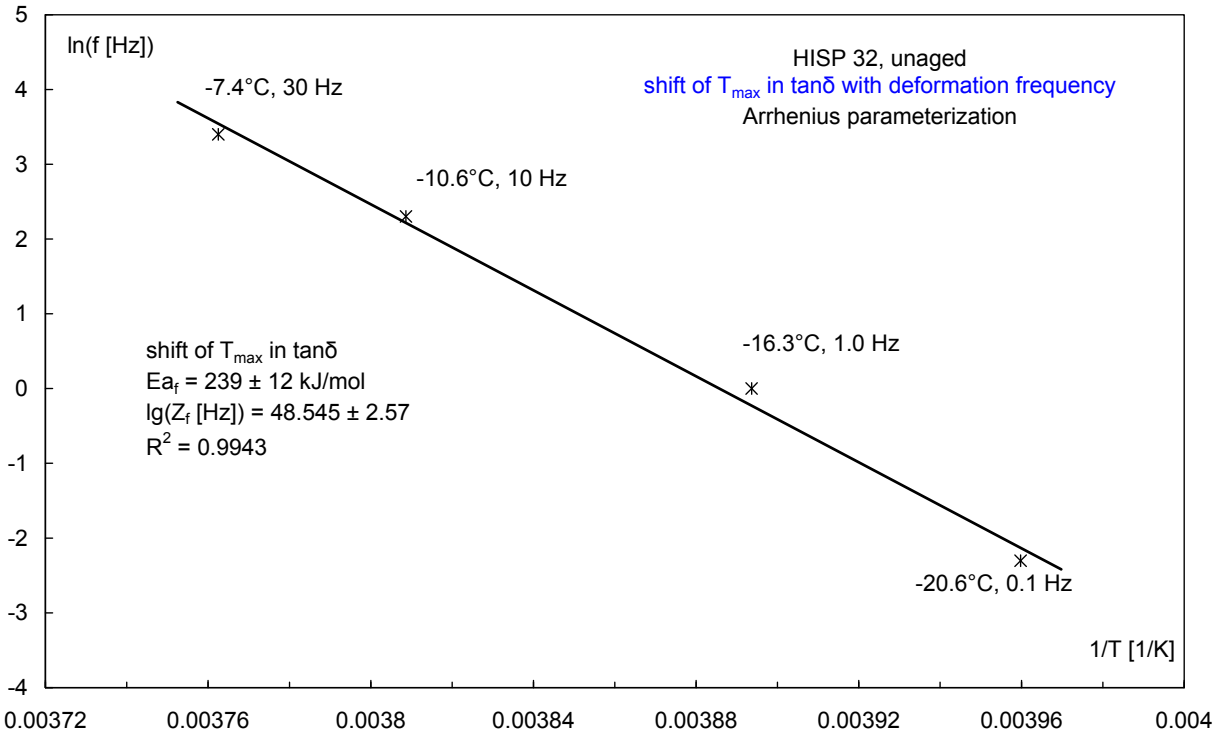

Figure 24: Arrhenius plot of the frequency shift of the T_{max} of the loss factor tanδ. The activation energy for the shift by strain rate is 239 kJ/mol.

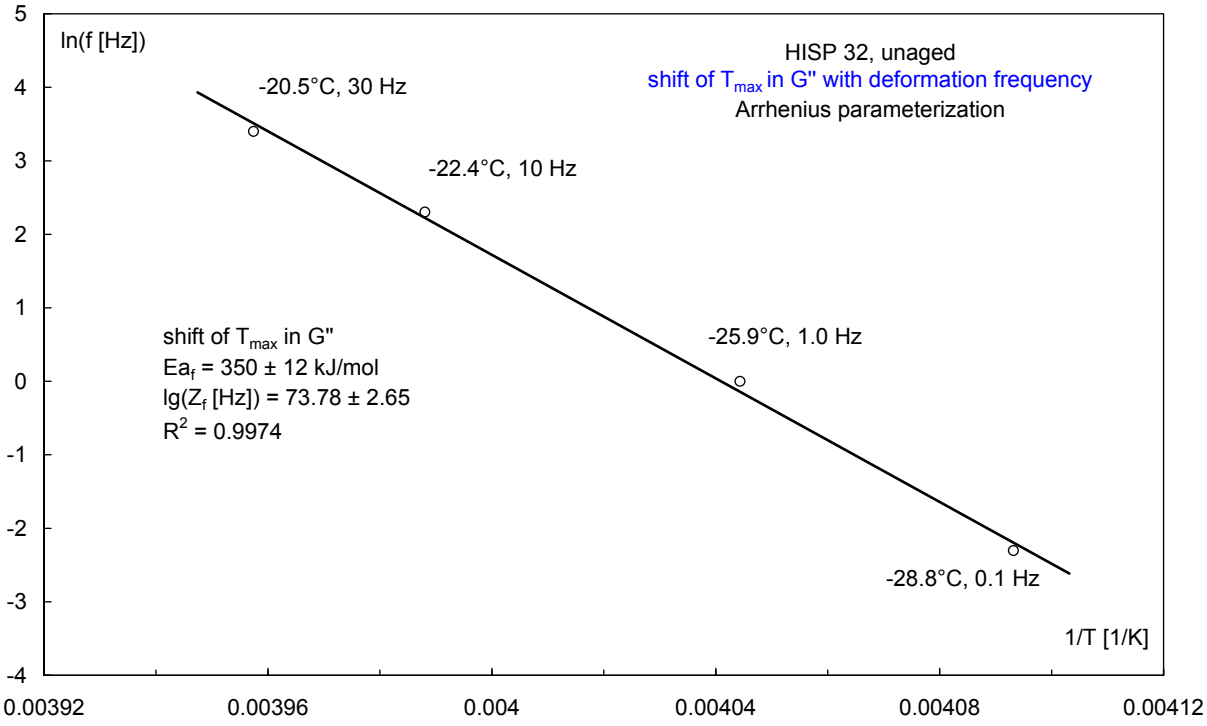

Figure 25: Arrhenius plot of the frequency shift of the T_{max} of the shear loss modulus G". High interaction energies in the already glassy state are reflected by the high activation energy of 350 kJ/mol.

This frequency dependence of the T_{max} values can formally be described with an Arrhenius expression in the way shown in Eq.(11). Here the deformation frequency is formally a rate constant.

$$f = Z_f \cdot \exp\left(-Ea_f / R / T_{max}\right) \qquad (11)$$

It is assumed that this process is thermally activated. This is insofar correct that interaction energies have to be overcome in order that the molecules get free to reorient. The application of this parameterisation is shown in the Fig. 24 for the loss factor and in Fig. 25 for the loss modulus. In the figures and in Table 3 the corresponding activation energies are given. The one for the shift of the G" maximum is about 110 kJ/mol higher than for the shift of the tanδ maximum. This means the interaction energies are at these lower temperatures already much greater than at the temperature range of the molecular reorientation. This is the reason why at the maximum of G" the material is already in the glassy state and not in the main chain reorientational state.

To complete the stability assessment, the gas evolution of HISP 32 at 80°C is shown in Figure 26. It is clearly higher than that of ADN alone. Means higher reactivity in the formulation and ageing processes have to be expected.

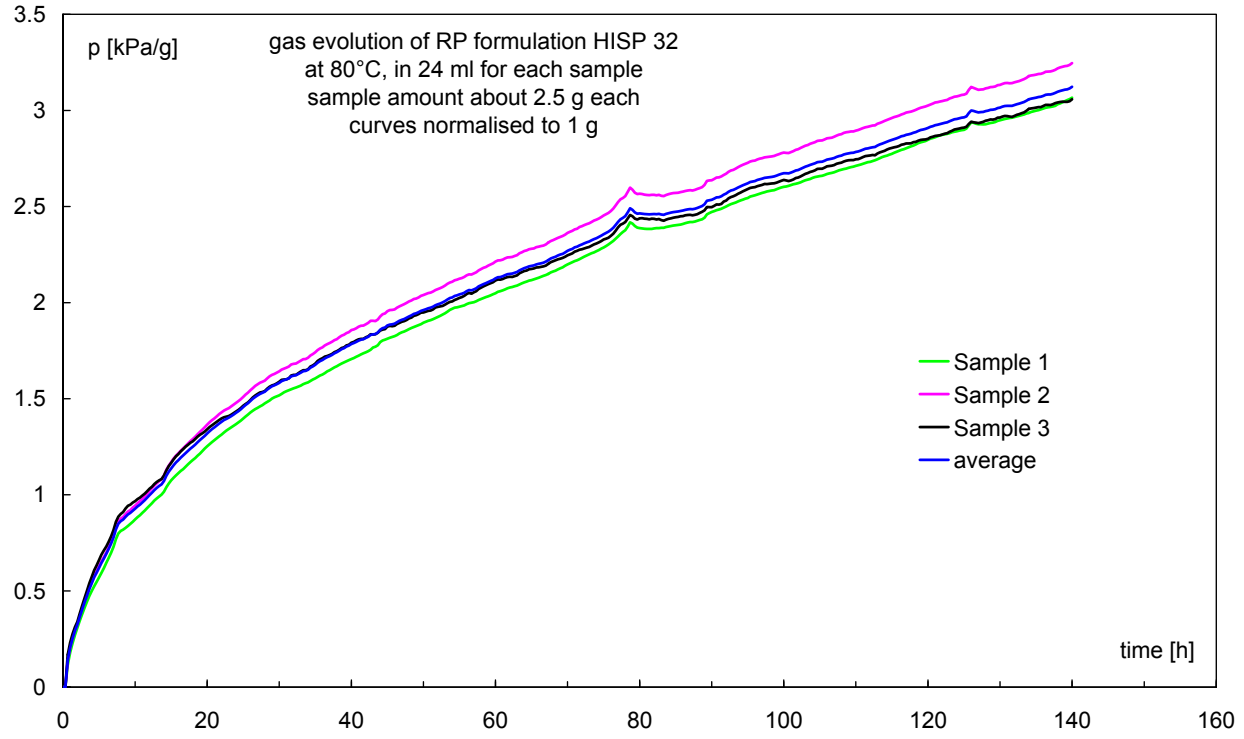

Figure 26: Gas evolution of RP formulation HISP 32 at 80°C. The normalised final gas volume is (0°C, 1 atm): 0.71 ml/g after 144 h.

4. Conclusions

ADN reacts with isocyanate and the gases N_2O, CO_2, nitrogen and also water are formed. This is very disadvantageous because of pore formation in the final cured propellant formulation. Therefore the conditions of the gas formation was investigated by IR- absorption and by following the total gas generation by a device used for determining VST, operating with pressure transducers. Measurement temperatures have been 50°C, 60°C and 70°C. The isocyanate used for this investigation was isophorone diisocyanate. By comparison of the gas evolution at these temperatures, a discrepancy occurred at 60°C: the experimental gas evolution was much faster than the one scaled from 50°C to 60°C. On the other hand scaling the gas evolution at 50°C to 70°C a coincidence was found with the measured data at 70°C. This means the anomalous decomposition of ADN occurred. The problem with gas formation is not avoidable. But at low curing temperatures and using cure catalysts the pore formation could be suppressed sufficiently not disturbing the burning behaviour of the propellant.

The so-named HISP 32 propellant, containing ADN, Al and GAP binder, was further investigated to characterize its glass-rubber transition. For this dynamic mechanical analysis (DMA) in torsion mode was employed and the loss factor curve ($\tan\delta = G''/G'$) was analysed in terms of binder parts with different reorientational behaviour during the transition from glassy to rubbery state. The shape of the loss factor is composed of two transitions: the one at lower temperatures originates from the undisturbed binder part and the one on the higher temperature side is caused by mobility restrictions exerted on the binder by the fillers ADN and Al powder. This is in agreement with findings from other GAP and GAP-ADN formulations. The perspective is that the different binder parts have different sensitivity to external loads as ageing and strain rate. The loss factor region is much more strain rate sensitive than the maximum of the loss modulus. This means at

typical in-service loads of rocket motors with strain rates corresponding to 100 to 1000 Hz the glass-rubber transition is shifted significantly to positive temperatures.

Abbreviations

ADN	ammonium dinitramide
AN	ammonium nitrate
AP	ammonium perchlorate
ARES™	Advanced Rheometric Expansion System. Manufactured by the Rheology unit of Rheometric Scientific Inc.; now belonging to Waters Inc., BU TA Instruments, Newcastle, Delaware, USA.
BPS	Bis-(propargyl) succinate, curing agent using 1,3 dipolar reaction between ethin bonds and azide groups; cross-linking is not really controllable along the GAP chains.
BLC	baseline correction (of loss factor)
DMA	Dynamic Mechanical Analysis
DSC	Differential Scanning Calorimetry
E305	diisocyanate based on HDI (hexane diisocyanate) and glycol, Desmodur™ type
EGA	evolved gas analysis
EMG	exponentially modified Gauss distribution
G*	Complex shear modulus; $G^* = G' + i \cdot G''$; $\lvert G^* \rvert = (G'^2 + G''^2)^{0.5}$
G'	storage shear modulus
G''	loss shear modulus
GAP	Glycidyl Azide Polymer, hydroxyl-terminated, binder pre-polymer
GRT	glass-rubber transition, occurs in elastomers, temperature induced
GvH	generalized van't Hoff rule
HISP	High Performance Solid Propellants for In-space Propulsion
HISP 32	Propellant formulation of Fraunhofer ICT; based on 60 mass-% bimodal ADN (208µm and 55µm), 16 mass-% Al (18µm), 24 mass-% GAP diol binder and combined BPS and isocyanate curing using Desmodur™ E305, curing catalyst DBTL.
HNF	hydrazinium nitroformate
HTPB	hydroxyl-terminated polybutadiene, binder pre-polymer
IPDI	isophorone diisocyanate
tanδ	loss factor, $\tan\delta = G''/G'$
$T_{g,DSC,h}$	Glass-rubber-transition temperature, determined by DSC at heating rate h (for clear information h has to be reported).
$T_{g,DMA,f}$	Glass-rubber-transition temperature, as maximum of loss factor, determined by DMA at deformation frequency f (for clear information f has to be reported).
VST	Vacuum Stability Test, performable by Hg-manometer apparatus or with pressure transducer apparatus.

Chemical formulas

CO_2	carbondioxide
CO	carbonmonoxide
N_2O	dinitrogenoxide, N=N=O, N≡N-O
N_2	nitrogen, N≡N

NO_2	nitrogendioxide
NH_3	ammonia
R-NCO	isocyanate, R-N=C=O
H_2O	water
ClO_4^-	perchlorate anion
$N(NO_2)_2^-$	dinitramine anion
$NH_4{\cdot}NO_3$	ammonium nitrate
$NH_4{\cdot}NO_2$	ammonium nitrite, instable decomposes to water and nitrogen
$NH_4{\cdot}N(NO_2)_2$	ADN, ammonium dinitramide
HDN	dinitramine acid

Companies and testing standards

ICT	Fraunhofer ICT, Pfinztal, Germany
OZM	OZM Research s.r.o.; Blížňovice 32; 538 62 Hrochův Týnec; www.ozm.cz
Rheometric	Rheometric Scientific Inc.; 1 Possumtown Road, Piscataway, NJ, USA; the Rheology unit, which manufactured the rheometers, belongs now to Waters Inc., BU TA Instruments, Newcastle, Delaware, USA.
STANAG	Standardization Agreement (related to NATO and PfP) NATO Standardization Agreement (NATO STANAG) 4582 Edition 1. '*Explosives, Nitrocellulose Based Propellants, Stability Test Procedure and Requirements Using Heat Flow Calorimetry'.* Military Agency for Standardization, NATO Headquarters, Brussels, Belgium.
AOP	Allied Ordnance Publication (related to NATO and PfP) NATO Allied Ordnance Publication (NATO AOP) 48, edition 2. *Explosives, Nitrocellulose-based Propellants, Stability Test Procedures and Requirements Using Stabilizer Depletion*. Military Agency for Standardisation, NATO Headquarters, 1110 Brussels, Belgium.

References

/1/ United States Environmental Protection Agency,
Perchlorate Treatment Technology Update.
http://www.epa.gov/tio/download/remed/542-r-05-015.pdf, May, **2005**.

/2/ B. Aas, M.A. Kettner, Th.M. Klapötke, M. Suceska, Ch. Zoller.
Asymmetric Carbamate Derivatives Containing Secondary Nitramine, 2,2,2-Trinitroethyl, and 2-Fluoro-2,2-dinitroethyl Moieties.
Eur. J. Inorg. Chem. DOI:10.1002/ejic.201301114, 35, 6028–6036, **2013**.

/3/ Q.J. Axthammer, Th.M. Klapötke, B. Krumm, R. Moll, S.F. Rest.
The Energetic Nitrocarbamate O2NN(H)CO[OCH2C(NO2)3] Derived from Phosgene.
Z. Anorg. Allg. Chem. 640, 76–83, **2014**.

/4/ Charles C. Lovenberg, George Svabeda.
Evaluation of bis (trinitroethyl) nitramine (BTNEN) as a substitute for cyclotrimethylenen-trintramine (RDX) in Composition A.
Naval Ordnance Laboratory, White Oak, MD, USA. Accession Number: AD0007458, 15 April **1952**.

/5/ Manfred A. Bohn
Review of some peculiarities of the stability and decomposition of HNF and ADN.
In: Proceedings of the 18th Seminar New Trends in Research of Energetic Material, University of Pardubice, pages 4 to 25. Czech Republic, 15-17 April **2015.**

/6/ Manfred A. Bohn
Review of some peculiarities of the stability and decomposition of HNF and ADN.
Paper on the Europyro 2015, held in conjunction with the 41st International Pyrotechnics Seminar. Seminar proceedings on USB-Stick, Session S1C, 'Energetic materials and molecules', page 100 to 119, in global pdf file '1361491_AF3P_Europyro.pdf'. Toulouse, France, May 4-7, **2015**.

/7/ H. Bathelt, F. Volk, M. Weindel.
The ICT Thermochemical Data Base.
Proc. 30th International Annual Conference of ICT, pp 56-1 to 56-12. Karlsruhe, Germany. June 29 - July 2, **1999**. Meanwhile available in new version **2008**.

/8/ M.J. Tummers, A.E.D.M. van der Heijden, E.H. van Veen.
Selection of burning rate modifiers for hydrazinium nitroformate.
Combustion and Flame 159, 882–886, **2012.**

/9/ G.B. Manelis.
Thermal decomposition of dinitramide ammonium salt.
Paper 15 in Proceed. of the 26th Internat. Annual Conference of ICT 1995, pages 15-1 to 15-17, July 4-July 7, **1995**, Karlsruhe, Germany. ISSN 0722-4087. Fraunhofer-Institut für Chemische Technologie (ICT), D-76318 Pfinztal-Berghausen, Germany.

/10/ Manfred A. Bohn.
Prediction of equivalent time-temperature loads for accelerated ageing to simulate preset in-storage ageing and time-temperature profile loads.
Paper 78, pages 78-1 to 78-28 in Proceedings of the 40th International Annual Conference of ICT on 'Energetic Materials – Characterization, Modelling, Validation', June 23 to 26, **2009**, Karlsruhe, Germany. ISSN 0722-4087. Fraunhofer-Institut für Chemische Technologie (ICT), D-76318 Pfinztal-Berghausen. Germany.

/11/ Manfred A. Bohn.
Generic formulation of performance assessment quantities for stability, compatibility and ageing of energetic materials.
Paper 59, pages 59-1 to 59-34 in Proceedings of the 43rd International Annual Conference of ICT on 'Energetic Materials – Synthesis, Characterisation, Processing', June 26 to 29, **2012**, Karlsruhe, Germany. ISSN 0722-4087. Fraunhofer-Institut fuer Chemische Technologie (ICT), D-76318 Pfinztal. Germany.

/12/ Sara Cerri, Manfred A. Bohn, Klaus Menke, Luciano Galfetti.
Ageing of HTPB/Al/AP rocket propellant formulations investigated by DMA measurements. Propellants Explosives Pyrotechnics **2013**, 38, 190 – 198.

/13/ Manfred A. Bohn and Sara Cerri.
Molecular mobility in binder systems.
Paper 96, pages 96-1 to 96-33 in Proceedings of the 42nd International Annual Conference of ICT on 'Energetic Materials – Modelling, Simulation and Characterisation of Pyrotechnics, Propellants and Explosives', June 28 to July 1, **2011**, Karlsruhe, Germany. ISSN 0722-4087. Fraunhofer-Institut für Chemische Technologie (ICT), D-76318 Pfinztal. Germany. Version CD-Proceedings.

/14/ Manfred A. Bohn, Günter Mußbach, Sara Cerri.
Influences on the loss factor of elastomer binders and its modelling.

Paper 60, pages 60-1 to 60-43 in Proceedings of the 43rd International Annual Conference of ICT on 'Energetic Materials – Synthesis, Characterisation, Processing', June 26 to 29, **2012**, Karlsruhe, Germany. ISSN 0722-4087. Fraunhofer-Institut fuer Chemische Technologie (ICT), D-76318 Pfinztal. Germany.

/15/ Sara Cerri, Manfred A. Bohn, Klaus Menke, Luciano Galfetti.
Aging of ADN Rocket Propellant Formulations with Desmophen®-Based Elastomer Binder.
Propellants, Explosives, Pyrotechnics 39, 526–537, **2014**. doi: 10.1002/prep.201300124.

/16/ Tijen Seyidoglu, Manfred A. Bohn.
Modelling of Loss Factor Curves Obtained by Torsion-DMA of HTPB and GAP Based Binders manufactured with Different Curing Agents and Plasticizers.
Paper 118, pages 118-1 to 118-26 in Proc. of the 46th International Annual Conference of ICT on 'Energetic Materials – Performance, Safety and System Applications', June 23 to 26, **2015**, Karlsruhe, Germany. ISSN 0722-4087. Fraunhofer-Institut fuer Chemische Technologie (ICT), D-76318 Pfinztal, Germany.

/17/ Tijen Seyidoglu, Manfred A. Bohn.
Characterization of Butacene® Based Composite Propellants by Loss Factor Curves Determined with DMA.
Paper on the Europyro 2015, held in conjunction with the 41st International Pyrotechnics Seminar. May 4-7, **2015**, Toulouse, France.